CrossMark

Urban Multi-scale Environmental Predictor (UMEP): An integrated tool for city-based climate services

Fredrik Lindberg [a, *], C.S.B. Grimmond [b, *], Andrew Gabey [b], Bei Huang [b, c], Christoph W. Kent [b], Ting Sun [b], Natalie E. Theeuwes [b], Leena Järvi [d], Helen C. Ward [b, e], I. Capel-Timms [b], Yuanyong Chang [f], Per Jonsson [g], Niklas Krave [a, b], Dongwei Liu [f], D. Meyer [b], K. Frans G. Olofson [a], Jianguo Tan [h], Dag Wästberg [g], Lingbo Xue [b, i], Zhe Zhang [b, j]

[a] Department of Earth Sciences, University of Gothenburg, Gothenburg, Sweden
[b] Department of Meteorology, University of Reading, Reading, United Kingdom
[c] Department of Hydraulic Engineering, Tsinghua University, Beijing, China
[d] Department of Physics, University of Helsinki, Finland
[e] Institute of Atmospheric and Cryospheric Sciences, University of Innsbruck, Innsbruck, Austria
[f] Shanghai Institute of Meteorological Science, Shanghai Meteorological Service, China
[g] Tyréns AB, Gothenburg, Sweden
[h] Shanghai Climate Centre, Shanghai Meteorological Service, China
[i] Information Center, Yangzhou University, China
[j] School of Environment and Sustainability, University of Saskatchewan, Saskatoon, Canada

ARTICLE INFO

ABSTRACT

UMEP (Urban Multi-scale Environmental Predictor), a city-based climate service tool, combines models and tools essential for climate simulations. Applications are presented to illustrate UMEP's potential in the identification of heat waves and cold waves; the impact of green infrastructure on runoff; the effects of buildings on human thermal stress; solar energy production; and the impact of human activities on heat emissions. UMEP has broad utility for applications related to outdoor thermal comfort, wind, urban energy consumption and climate change mitigation. It includes tools to enable users to input atmospheric and surface data from multiple sources, to characterise the urban environment, to prepare meteorological data for use in cities, to undertake simulations and consider scenarios, and to compare and visualise different combinations of climate indicators. An open-source tool, UMEP is designed to be easily updated as new data and tools are developed, and to be accessible to researchers, decision-makers and practitioners.

1. Introduction

Urban environments are particularly vulnerable to high impact weather given the high population densities in many cities and the associated assets and infrastructure (e.g. as evidenced by the impacts of Hurricane Sandy on New York City, Solecki, 2015). With weather extremes frequently exceeding climate records, and with urban areas growing rapidly, the ability to deliver city-based climate services to those operating and planning different aspects of city life (transport, energy demand, water supply etc.) is critical (Horton et al., 2016; Baklanov et al., 2017). A common toolbox, accessible to researchers, decision-makers and practitioners, offers great potential for better informed climate-related decisions in cities.

Scientists and practitioners from a broad range of disciplines including architecture (e.g. Ren et al., 2011), climatology (e.g. Eliasson, 2000), planning (e.g. Alcoforado et al., 2009), engineering and geography have long been interested in how weather and climate affects cities and their occupants (Baklanov et al., 2017). However, the development and adoption of city-based climate services, which require production, translation, transfer,

---

* Corresponding authors.
  E-mail addresses: fredrikl@gvc.gu.se (F. Lindberg), c.s.grimmond@reading.ac.uk (C.S.B. Grimmond).

communication, and use of climate knowledge and information for urban planning, building design and the operation of cities, is not straight-forward (Chrysoulakis et al., 2013; Grimmond et al., 2014; Masson et al., 2014; Baklanov et al., 2017). Appropriate input data (surface and atmospheric) can be challenging to access and specialist formats often make them inaccessible to many end-users (Grimmond, 2013). Communication between producers and users of climate services has been poor, with outputs often not easily interpretable by non-specialists. Tools that are more user-friendly, and are technically and economically accessible to users, are needed to improve communication across disciplines, researchers and users; to better identify user needs; to ensure common assumptions across models; to build capacity to address urban climate and weather concerns; and transfer research into practice. Past initiatives have tended to focus on specific processes (e.g. Herbert et al., 1998) or restricted spatial or temporal scales (e.g. Bruse and Fleer, 1998), with applications most often intended for specialist researchers. Many of these studies have focused on water and waste water management (e.g. Paton et al., 2014; Saagi et al., 2017) and not on integrated hydro-climatological models appropriate for application at multiple scales (neighbourhood to city) which account for feedbacks and complex interactions (for example the effect of water on heat exchanges as well as on flooding).

Here we introduce UMEP (Urban Multi-scale Environmental Predictor), an integrated tool for urban climatology and climate-sensitive planning applications. While elements of UMEP have been presented elsewhere (see further discussion below and summary in Table 1), this is the first full description of UMEP and its potential across a broad range of applications.

In its current form, the tool can be used for applications related to outdoor thermal comfort, urban energy consumption and climate change mitigation. UMEP consists of a coupled modelling system which combines state-of-the-art 1-D and 2-D models with systems to input data from multiple sources, formats and at different temporal and spatial scales, and to generate output as data, graphs and maps. An important feature of UMEP is its ability to couple relevant processes and to use common data across a range of applications. Here the basic structure of UMEP is described, followed by examples of applications to illustrate the potential of this tool.

2. UMEP overview

UMEP is being developed as a community, open-source tool to enable its use without restriction with respect to cost, license or rights issues. Users are encouraged to contribute to the tool to enhance and extend its capabilities. One of its major features is the ability for users to interact with spatial information to determine model parameters, and to edit, map and visualise inputs and results. For this reason, the software is written as a plug-in to QGIS, a cross-platform, free and open source desktop geographic information system (GIS) application (QGIS Development Team, 2017).

UMEP has three main elements (Fig. 1): *pre-processor* (for inputs of meteorological and surface information); *processor* (modelling system e.g. Urban Land Surface Models, ULSM); and *post-processor* (tools to analyse the outputs (individual case and ensemble, indicators of uncertainty, user applications *etc.*)). Each element is described briefly in Table 1, with more complete details presented in the online manual (http://www.urban-climate.net/umep/UMEP). UMEP allows users to: integrate atmospheric and surface data from multiple sources; take meteorological data measured at 'standard' sites and adapt them to be representative of the urban environment; use reanalysis or climate prediction data; and compare and visualise results or scenarios for different climate indicators of interest (heat indices, intense precipitation, water/energy demand). This all can be done at a range of spatial scales consistent with end-users' needs and interests (Table 1). To aid uptake and use of the model, and to develop capacity in urban modelling more generally, a series of tutorials have been developed (http://www.urban-climate.net/umep/UMEP_Manual#Tutorials).

One key contribution of UMEP is to facilitate the preparation of input data required for City-Based Climate Services (CBCS). UMEP provides both guidance and tools that enable the preparation and manipulation of data (Table 1). This is particularly important as most end-users are familiar with some, but not the full spectrum of, data needed for applications. For example, planners are knowledgeable about building heights, materials and their spatial arrangement (i.e. urban surface data) and often have GIS skills, but they may not necessarily have detailed knowledge of meteorological data. Equally, those knowledgeable of the latter may not be expert of the former. Although remotely sensed data may play a very useful part in CBCS, these data may require further processing to be applicable in urban areas. UMEP has been designed to enhance their integration. The tools within UMEP can also be used to provide data to export to other more complex weather, climate, hydrological, environment modelling systems. Alternatively, data from more complex models may be imported into UMEP.
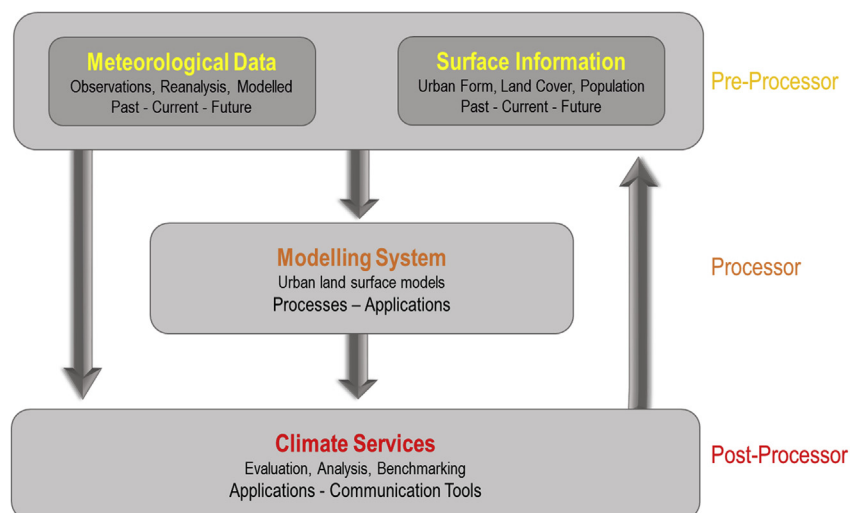

Fig. 1. Structure of UMEP (Urban Multi-scale Environmental Predictor).

Table 1
Description of UMEP components and scales of applicability [C: city; L: local (neighbourhood); M: micro (e.g. street canyon, park)], with an example of where their application may be useful. Those components with post-processing visualization tools are indicated with (*), benchmarking or other statistics are indicated with (+), and components described in detail in the text with (#). Note, the micro scale applications are usable across a whole city, but are likely to be computer intensive.

	Component	Scales	Description	Example Applications	Key References
(a) Pre-processor					
Meteorological data	Prepare existing data#	C/L/M	Formats meteorological data for input to the models, dealing with missing data	Local weather station data can be manipulated into a standard format and subjected to basic quality control	n/a
	Download Data (WATCH)#	C/L	Downloads climate re-analysis data; modifies it for use in an urban context, representative of the local scale	If local meteorological data are unavailable, allows reanalysis data for land surface modelling to be used	Weedon et al. (2011, 2014) Kokkonen et al. (2017) Ward et al. (2017a,b)
Spatial Data	Spatial Data Downloader#	C/L/M	Downloads spatial data from public servers	If spatial population data within a city are unavailable, they can be downloaded from world-wide online dataset	n/a
	Tree Generator	C/L/M	Creation/manipulation of 3D vegetation data	Influence of vegetation on thermal comfort and energy exchanges in a city	n/a
	LCZ Converter	C/L	Allows morphometric parameters and land cover fractions (see Table 4) to be calculated from Local Climate Zone (LCZ) maps generated by WUDAPT (http://www.wudapt.org/).	Generates surface input data for city- to neighborhood-scale modelling.	Stewart and Oke (2012) Ching et al. (2017)
Urban geometry	Sky View Factor	L/M	Amount of the hemisphere with restricted view of the sky	Solar access, urban heat island, thermal comfort modelling.	Lindberg and Grimmond (2011a,b)
	Wall Height Aspect#	L/M	Height and orientation of buildings and walls	Solar access, urban heat island, thermal comfort modelling.	Lindberg et al. (2016a)
Urban land cover	Land Cover Reclassifier	C/L/M	Geodata can be translated into the land cover classes used by all the models	Remote sensing and other geodata sources (e.g. MODIS classes) can be modified for use with models and made appropriate for a local area.	n/a
	Land Cover Fraction (point)	L/M	Surface cover fractions are determined for an area (circle of selected diameter) or specific directions (Table 4)	Analysis and characterization of a measurement site	n/a
	Land Cover Fraction (grid)#	C/L	As above, but a grid is used to determine fractions for multiple areas.	Data input for an extensive area for modelling.	n/a
Urban Morphology	Morphometric Calculator (point)	L/M	Morphometric parameters (Table 4) are determined for an area (circle of selected diameter) or specific directions can be used.	Interpretation of a measurement location in terms of surface roughness	Kent et al. (2017a,b) Table 4
	Morphometric Calculator (grid)#	C/L	As above, but a grid is used to determine parameters for multiple areas.	Data input on surface roughness for an extensive area for modelling	Kent et al. (2017a,b) Table 4
	Source Area (point)	L/M	As above, but determined for an area derived from source area models.	Interpretation of observations, investigation of potential siting of instruments	Kormann and Meixner (2001) Kljun et al. (2015) Kent et al. (2017a,b)
	SUEWS Prepare#	C/L	Prepares input data for the SUEWS model (processor) based on information derived from other pre-processing tools within UMEP.	For extensive analysis using SUEWS, input forcing data and derived spatial information needed can be prepared	n/a
(b) Processor					
Thermal Comfort	ExtremeFinder#	C	Finds extreme high and extreme low events (e.g. heat waves or cold waves) in meteorological time series data (Table 2).	Identification of extreme temperatures from a long climate record.	See Table 2
	Mean Radiant Temperature (SOLWEIG)*#	L/M	SOLWEIG estimates spatial (2-D) variations of 3-D radiation fluxes and the mean radiant temperature (T_{mrt}) in complex urban settings. Both 3D vegetation (trees and bushes) as well as ground cover variations are currently considered in the model.	T_{mrt} is an important meteorological variable governing the human energy balance and thermal comfort outdoors, especially during clear and calm summer days (Mayer and Höppe, 1987)	Lindberg et al. (2008) Lindberg and Grimmond (2011a,b), Lindberg et al. (2016b)
Urban Energy Balance	Anthropogenic Heat (Q_F) (LQF)#	C/L/M	Globally applicable method (low spatial resolution) to calculate Q_F	Quantifies contributions to energy budget from building energy use and road traffic.	Allen et al. (2011) Lindberg et al. (2013a) Gabey et al. (2017)
	Anthropogenic Heat (Q_F) (GQF)#	C/L	Locally applicable method (high spatial resolution) to calculate Q_F	Quantifies contributions to energy budget from road traffic, residential and non-residential building energy use, with different fuels and vehicle types considered.	Iamarino et al. (2012) Gabey et al. (2017)
	Urban Energy and Water Balance (SUEWS; Simple)* #	C/L	Urban land surface model that allows radiation, energy and water fluxes to be calculated for a single point or area.	Simulations of evaporation and heat fluxes for a neighborhood or across a city	Järvi et al. (2011, 2014) Ward et al. (2016, 2017b)
	Urban Energy and Water Balance (SUEWS; Advanced)*#	C/L	As above, but for multiple areas (e.g. a city with 1000s of grid squares, or local planning zones (of any shape).	Assessment of future city plans and impacts of drought, heatwaves, water management, green infrastructure.	Table 3

Table 1 (*continued*)

	Component	Scales	Description	Example Applications	Key References
Solar Radiation	Solar Energy on Building Envelopes (SEBE) *#	L/M	Shortwave irradiance on ground, roofs and building walls is estimated based on high resolution Digital Surface Models (DSMs) and input meteorological forcing data.	Potential for energy production, resource planning.	Lindberg et al. (2016b)
	Daily Shadow Patterns	L/M	Shadow maps are derived from buildings and 3D vegetation.	Impact of building form and vegetation on energy production, outdoor thermal comfort. Planning of parks and outdoor spaces	Lindberg and Grimmond (2011a,b), Ratti and Richens (1999)
(c) Post-processor					
	SEBE (Visualization)	L/M	Visualization of solar irradiation on building envelopes (roofs and walls)	Identify areas of good or poor potential for generation of solar energy if panels were installed	n/a
	SOLWEIG Analyzer#+	L/M	SOLWEIG output: point (temporal), model domain (spatial/temporal)	Identify: potential hazard areas; potential sites for outdoor activities (e.g. café, park).	n/a
	SUEWS Analyzer#+	C/L	SUEWS output: point (temporal), model domain (spatial/temporal)	Comparison of indicators under different planning scenarios through time and as maps	Ward and Grimmond (2017)
	Benchmarking+	C/L/M	Statistical tool to compare different datasets	Model evaluation	n/a

Table 2
The heat-cold- wave indices used in UMEP- **ExtremeFinder**.

Extreme Event	Reference	Index description
Heat-wave	Meehl and Tebaldi (2004)	Longest period when maximum temperature is above the 97.5th percentile for at least 3 days; average daily maximum temperature across the event is over the 97.5th percentile; and all days are above the 81st percentile.
	Fischer and Schär (2010)	Periods of at least 6 days where maximum temperature exceeds the calendar day 90th percentile.
	Vautard et al. (2013)	Periods of various length when daily mean temperature is above the 90th percentile.
	Schoetter et al. (2014)	At least 3 days above the 98th percentile of maximum temperature.
Cold -wave	Keevallik and Vint (2015)	*Cold night*: temperature lower than 10th percentile of daily minimum temperatures calculated for a 5-day window centered on each calendar day in dataset; *Cold wave*: six consecutive cold nights.
	Srivastava et al. (2009)	Minimum temperature is below the normal temperature by 3 °C or more, consecutively for 3 days or more.
	Busuioc et al. (2010) Cited by Micu (2012)	At least 6 consecutive days with negative deviations of at least 5 °C from the normal value of each calendar day.

UMEP has a broad range of capabilities (Table 1). Each of its elements may be used independently or in varying combinations. Users may be interested in the output from tools that are provided in the pre-processor for other modelling applications (e.g. in generating urban surface information or standardised meteorological fields) or in applications that require a chain of tools to provide climate indicators for decision making. As many of the individual tools, as well as their evaluations, have been described in disciplinary focussed papers (see Table 1 references), here we present a range of examples, each of which requires the use of several tools to obtain a solution.

3. UMEP applications

In this section examples of applications are presented to illustrate UMEP's potential, specifically in the identification of heat waves and cold waves in cities (**ExtremeFinder**) (bold is used hereafter to indicate the component of the UMEP plug-in tool) ; the implications of green infrastructure on runoff (**SUEWS**); microscale heat stress (**SOLWEIG**); solar energy production (**SEBE**); and sources of anthropogenic (human-generated) heat (**LQF**, **GQF**). Each application draws on different combinations of UMEP tools.

3.1. Application example 1 - identification of extreme thermal conditions

For many urban planning and human health applications,

extreme meteorological conditions are of interest and concern. To identify these extremes, analysis of a long climatological record is required (Table 2). However, if such data are not available for the area of interest, UMEP allows the user to draw on the reanalysis dataset WATCH Forcing Data ERA-Interim (WFDEI) (Dee et al. 2011; Weedon et al., 2011, 2014). This product was selected as it was designed to be used for hydrological and land-surface modelling for climate purposes and has been used in several cities around the world to explore variations in energy flux partitioning (Best and Grimmond, 2016).

To determine the extreme thermal conditions for a site, the first step is to use the UMEP **Download data (WATCH)** (Table 1) to obtain a meteorological time series for the period and location of interest. These data can also be used for other UMEP applications (e.g. section 3.2). For example, they can be downscaled to the area of interest using the techniques of Best and Grimmond (2016) and Ward et al. (2017a,b) (Appendix 1).

Currently, **ExtremeFinder** provides four methods to identify heat-waves and three for cold-waves (Table 2), as there is no generally accepted definition of either phenomena (Robinson, 2001; Vaidyanathan et al., 2016) different percentiles are used to define extremes (e.g. Table 2). The thresholds for the extremes are based on fixed values or quantiles calculated from the meteorological time series. Use of a time series spanning decades is therefore recommended. The user can modify the fixed thresholds and quantiles (http://urban-climate.net/umep/UMEP_Manual#Outdoor_Thermal_Comfort:_ExtremeFinder). Daily values are then evaluated

to determine if an extreme event has occurred. **ExtremeFinder** identifies the dates and daily maximum (average or minimum) temperatures of all extreme high (low) events during the period of interest (Fig. 2, yellow boxes) based on the criteria set out by the method chosen.

3.2. Application example 2 - urban energy and water balance fluxes

Energy and water balance fluxes are critical to surface-atmosphere interactions in an urban area. The impact of extreme conditions (heat waves, droughts, floods etc.) are influenced by the state of the urban environment prior to these events, with the urban energy and water balance varying with different neighbourhood (local-scale) characteristics. The Surface Urban Energy and Water balance Scheme (SUEWS) is an urban land-surface model included in the processing part of UMEP (Table 1). The model simulates the urban radiation, energy and water balances using commonly measured meteorological variables and information about the surface cover. SUEWS is applicable at the neighborhood to city scale. In UMEP SUEWS is uncoupled, i.e. advection between grids is not accounted for. UMEP allows SUEWS to be run as a standalone model, or UMEP can provide the appropriate parameters for the use of SUEWS within a 3-D model meso-scale model such as WRF (Dudhia, 2014). The parameters calculated with UMEP tools can provide the input parameters to a wide range of urban land surface models (either standalone versions SURFEX (Masson et al., 2013), JULES (Best et al., 2011), CLM (Lawrence et al., 2011), SLUCM (Kusaka et al., 2001) or coupled to larger scale models).

SUEWS uses an evaporation-interception approach (Grimmond and Oke, 1991) for an area comprised of seven land cover types (water, buildings, grass, paved, bare soil, deciduous trees/shrubs and evergreen trees/shrubs). The state of each surface type at each time step is calculated from the running water balance of the canopy where the evaporation is calculated from the Penman-Monteith equation. The soil moisture below each surface type (excluding water) is considered. UMEP has the latest version of SUEWS (Ward et al., 2017a,b) accessible through two links:

a) **SUEWS Simple**: provides a useful starting place to introduce UMEP and SUEWS. Example data are provided so that users can explore the impact of modifying urban surface characteristics. With **SUEWS Simple**, the ULSM can be executed for a single location (area).

b) **SUEWS (Advanced)** provides a full version of the model appropriate for investigating both spatial and temporal variations of the urban energy balance.

The SUEWS model has been extensively evaluated for a variety of locations and situations worldwide (Table 3).

The workflow for an application utilizing SUEWS within UMEP is outlined in Fig. 3. Geodatasets that contain information about the urban environment are used with the pre-processor tools (Fig. 3, gray and yellow) to provide the required surface parameters. The model can be applied to areas of any shape, as in most cities planning units have known boundaries already available in vector polygon format (e.g. boroughs, wards). Alternatively, a square grid can easily be created in QGIS (Fig. 4a).

As land cover (Fig. 3) is a key variable for many calculations, a method to reclassify data is provided. The UMEP **Land Cover Reclassifier** enables land cover raster grids to be created from sources such as MODIS and then converted to the standard UMEP cover types (Table 4). Surface cover fractions are very important given differences in energy and water partitioning that result from underlying differences in moisture availability and surface properties.

Accessing reliable sources of land cover information to derive these parameters at the scale of interest remains a challenge. Crowd-sourced data sets such as OpenStreetMap (http://www.openstreetmap.org) and WUDAPT (http://www.wudapt.org/, see below) offer potential but may be incomplete or inconsistent. Other sources such as MODIS (https://terra.nasa.gov/about/terra-instruments/modis) are likely to be complete but give low spatial resolution at the sub-km scale. In addition, the number of human-altered (urban) classes from such data are limited (3 classes) and the discrimination between land cover classes needs to be made based on land use. In the example given here for central London, the land cover information (Fig. 4a) is derived from OS MasterMap® Topography Layer (Ordnance Survey, 2010). The **Land Cover Fraction (Grid)** tool is used to calculate grid-based land cover fractions (Tables 1 and 4) based on the land cover raster grid.

Morphometric parameters (Table 4) related to surface roughness can be obtained from the **Morphometric Calculator (Grid)** using digital surface models (DSM) (Fig. 4b). From these data, the zero-plane displacement (z_d), aerodynamic roughness length (z_0) and other geometric parameters such as mean roughness-element height and frontal area index are calculated (Table 4). The rationale behind the different methods, and a basis for selecting between
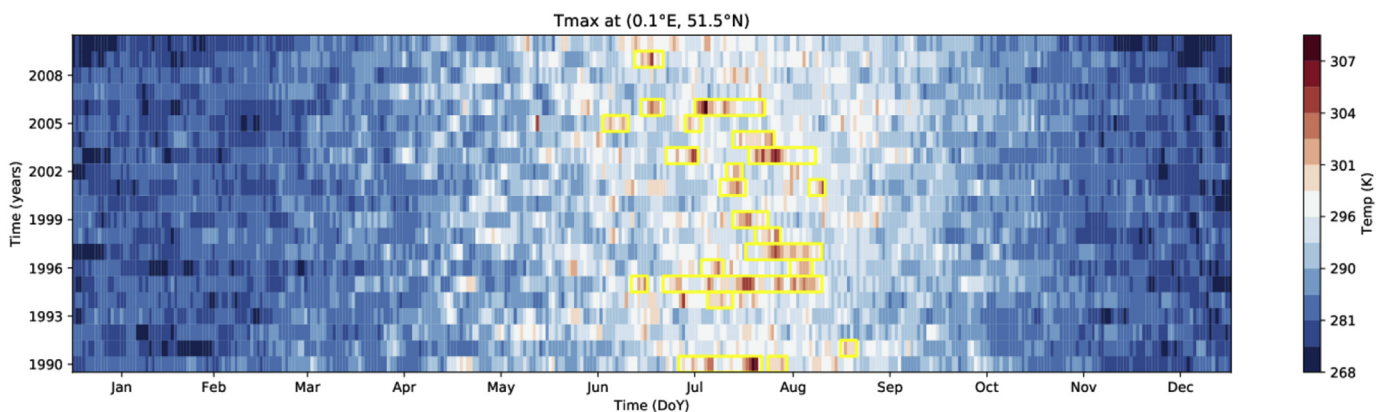

Fig. 2. After heat-wave or cold-wave conditions are identified with **ExtremeFinder,** a series of graphs are generated including the daily temperatures with the extreme periods indicated in yellow. In the example here, heatwaves are identified for London (yellow boxes) in the period 1990−2010 using the Meehl and Tebaldi (2004) method (Table 2). (For interpretation of the references to colour in this figure legend, the reader is referred to the web version of this article.)

Table 3
Studies that have evaluated and applied SUEWS (presented chronologically). Note other sub-component models have been evaluated and applied prior to these references.

City	Reference	Variables evaluated/application
Evaluation		
Vancouver, Canada	Järvi et al. (2011)	Water use, anthropogenic heat flux, radiation, sensible and latent heat fluxes, soil moisture, surface wetness
Los Angeles, USA	Järvi et al. (2011)	Radiation, sensible and latent heat fluxes
Helsinki, Finland	Järvi et al. (2014)	Radiation, sensible and latent heat fluxes, snowmelt, runoff, albedo, snow depth
Montreal, Canada	Järvi et al. (2014)	Radiation, sensible and latent heat fluxes, snowmelt, albedo, snow density, snow depth
Dublin, Ireland	Alexander et al. (2015, 2016a)	Radiation, sensible and latent heat fluxes
Sacramento, USA	Onomura et al. (2015)	Boundary layer height, sensible and latent heat flux
Hamburg, Germany	Alexander et al. (2016a)	Sensible and latent heat fluxes
Melbourne, Australia	Alexander et al. (2016a)	Sensible and latent heat fluxes
Phoenix, USA	Alexander et al. (2016a)	Sensible and latent heat fluxes
Swindon, UK	Ward et al. (2016)	Radiation, sensible and latent heat fluxes, soil moisture, surface wetness
London, UK	Ward et al. (2016)	Radiation, sensible and latent heat fluxes, soil moisture
Helsinki, Finland	Karsisto et al. (2015)	Radiation, sensible and latent heat fluxes, snow depth
Shanghai, China	Ao et al. (2016)	Radiation
Singapore	Demuzere et al. (2017)	Radiation, sensible and latent heat fluxes
Basel, Switzerland	Järvi et al. (2017)	Radiation, sensible and latent heat fluxes, snow depth
Minneapolis-Saint Paul, USA	Järvi et al. (2017)	Radiation, sensible and latent heat fluxes, snow depth
Application		
Helsinki, Finland	Nordbo et al. (2015)	Effect of surface cover resolution on SUEWS performance
Dublin	Alexander et al. (2016a,b)	Impact of urban development pathways on sensible and latent heat fluxes across the city of Dublin
Dublin, Ireland	Alexander et al. (2016b)	LCZ classification combined with SUEWS
Hamburg, Germany	Alexander et al. (2016b)	LCZ classification combined with SUEWS
Melbourne, Australia	Alexander et al. (2016b)	LCZ classification combined with SUEWS
Phoenix, USA	Alexander et al. (2016b)	LCZ classification combined with SUEWS
Porto, Portugal	Rafael et al. (2016)	Urban resilience measures under different climate scenarios
London, UK	Ward and Grimmond (2017)	Impact of urban development and climate mitigation measures on energy partitioning across Greater London

Table 4
Spatially related urban surface parameters determined by UMEP pre-processors.

Plug-in	Parameters	
Land Cover	Types: water, building, paved surfaces, bare soil, deciduous trees, evergreen trees, and grass surfaces	
	Plan area fraction; the combined fractions for a grid must sum to 1.	
Source area	Two source area models are included: Kormann and Meixner (2001), Kljun et al. (2015)	
Morphometric methods	H_{av} — average roughness-element height	**Methods for z_0 and z_d:**
	λ_p — plan area index	Rule of thumb (Grimmond and Oke, 1999)
	λ_f — frontal area index	Raupach (1994)
	H_{max} — maximum roughness-element height	Bottema and Mestayer (1998)
	σ_H — standard deviation of roughness-element heights	Macdonald et al. (1998),
	z_0 — Aerodynamic roughness length	Millward-Hopkins et al. (2011)
	z_d — zero-plane displacement	Kanda et al. (2013)
Wall Height and Aspect	Wall height	
	Aspect (orientation °)	
SVF Calculator	Sky View Factor (Values of 1 indicate complete sky access, 0 no sky access. Height of calculations can be varied)	

them, is outlined in Kent et al. (2017a,b). Parameters can be derived for the full surrounding area or for sectors reflecting different wind directions.

Applications which involve an assessment of the area surrounding a measurement point can use the **Source Area Model (Point)**. Currently, there are two turbulent flux source area models included within UMEP (Tables 1 and 3): the analytical model of Kormann and Meixner (2001) and Kljun et al.'s (2015) parameterisation of a Lagrangian stochastic particle dispersion model. These models indicate the probable surface area contributing to a turbulent flux measurement at a specific point in time and space with imposed boundary conditions (e.g. meteorological conditions, sources/sinks of passive scalars or surface characteristics). The results from these models facilitate interpretation of observations, enable improved evaluation of flux models, and/or allow assessments of the appropriateness of siting of new instrumentation (Fig. 5).

Population density (people per hectare) is used in the estimation of anthropogenic heat flux in SUEWS. If population density datasets are unavailable (e.g. as would be obtained from local census data), the **Spatial Data Downloader** can be used. This plug-in is directly connected to various Web Coverage Services (WCS) including global datasets on population density (http://urban-climate.net/umep/UMEP_Manual#Spatial_Data:_Spatial_Data_

Downloader). In the example given here, averaged population density between residential and working population is used (Fig. 4c). Such differentiations are very important in locations such as central London for anthropogenic heat flux calculations (Dong et al., 2017; Gabey et al., 2017).

Given the challenges of acquiring all the datasets needed (DEM, DSM, and land cover in Fig. 3), local climate zone maps (LCZ; Stewart and Oke, 2012) are included in UMEP. From these, a first estimate of input parameters for SUEWS can be made. In UMEP the LCZ maps from the WUDAPT database (www.wudapt.org; Ching et al., 2017) can be translated using the **LCZ Converter**. If more detailed information is available for specific areas, or becomes available subsequently (e.g. local high resolution DSMs), parameters can be updated.

The other major input to SUEWS is the meteorological forcing data (Table A1.1). Such data need to be for above the height of the roughness elements (trees, buildings). A common format is used in all UMEP models (Table A1.1). Most applications require a continuous gap-filled data set. For many urban applications, the start and finish of daylight savings is linked to important behavioural patterns (e.g. the shift of rush hour). Therefore, the individual models account for daylight savings if relevant (e.g. timing of anthropogenic energy use, irrigation). The **Preparing Existing Data** UMEP

tool (see Appendix 1) supports preparation of the meteorological data and conversion into the format used in all UMEP models.

Once all the required information is pre-processed, **SUEWS Prepare** can arrange the data so the model can be executed. **SUEWS Analyzer** (Fig. 3) allows spatial (Fig. 6a), temporal (Fig. 6b) and between variable (Fig. 6c) model results to be explored. In this example application, central London average daytime sensible heat fluxes (Q_H) for four-months period in 2015 are mapped (Fig. 6a), with detail of temporal variations of net all-wave radiation (Q^*) and Q_H for nine days for one area (grid ID 44) graphed (Fig. 6b). The relation between Q^* and Q_H for grid ID 44 for the whole time period (Fig. 6c) is also plotted.

To illustrate a hydrological application, to examine runoff generation in different planning scenarios, SUEWS was run for a highly built-up catchment area (24 ha) in Helsinki for 2010 (Fig. 6d–f). The planning scenarios considered the current land cover/use (base run), and a 10% and 30% increase in areal coverage of street trees and grass surfaces at the expense of paved surfaces (Fig. 6f). Results from these simulations indicate that the increase in the amount of street trees (i.e. areal fraction of street trees) is more effective in reducing surface runoff compared to an increase in grass surfaces (a 10% increase in street trees is more effective than a 30% increase in grass surfaces).

3.3. Application example 3 - mean radiant temperature

Temperature-related health problems are expected to increase with rising temperature in cities, especially during more extreme temperatures associated with heat waves. Mean radiant temperature (T_{mrt}) is one of the most important meteorological variables governing the human energy balance and thermal comfort outdoors, especially on clear and calm summer days (Mayer and Höppe, 1987). To provide estimates of thermal comfort/heat stress for people, **SOLWEIG** (SOlar and LongWave Environmental Irradiance Geometry model) can be used to calculate T_{mrt}. In **SOLWEIG**, both 3D vegetation (trees and bushes), as well as variations in ground cover, can be considered (Lindberg and Grimmond, 2011b; Lindberg et al., 2016b). SOLWEIG has been evaluated extensively and applied at urban locations worldwide (Table 5).

Table 5
Evaluation and application studies using the SOLWEIG model.

| City	Reference	Variables	Settings
Evaluation			
Gothenburg, Sweden	Lindberg et al. (2008)	Radiant fluxes and T_{mrt}	City square, courtyard
Gothenburg, Sweden	Lindberg and Grimmond (2011a)	Radiant fluxes and T_{mrt}	City square with tree
Kassel, Germany	Lindberg and Grimmond (2011a)	T_{mrt}	Street canyon
Freiburg, Germany	Lindberg and Grimmond (2011a)	T_{mrt}	Four urban sites
London, UK	Lindberg et al. (2016b)	Radiant fluxes and T_{mrt}	Different urban ground covers
Shanghai, China	Chen et al. (2016)	T_{mrt}	Very dense urban environment
Hong Kong, China	Lau et al. (2016)	T_{mrt}	Very dense urban environment
Application			
Gothenburg, Sweden	Thorsson et al. (2010)	Spatial and temporal T_{mrt}	Future climate scenarios
London, UK	Lindberg and Grimmond (2011b)	T_{mrt}	Intra-urban differences
Gothenburg, Sweden	Lindberg et al. (2013a,b)	Spatial T_{mrt}	Consideration of weather
Stockholm, Sweden	Thorsson et al. (2014)	T_{mrt}	Prediction of heat related mortality
Porto, Portugal	Lau et al. (2014)	T_{mrt}	Effects of urban geometry, climate change
Gothenburg, Sweden	Lau et al. (2014)	T_{mrt}	Effects of urban geometry, climate change
Frankfurt, Germany	Lau et al. (2014)	T_{mrt}	Effects of urban geometry, climate change
Berlin, Germany	Jänicke et al. (2016)	T_{mrt}	City-wide characteristics
Adelaide, Australia	Thom et al. (2016)	T_{mrt}	Influence of increasing tree cover
Gothenburg, Sweden	Lindberg et al. (2016b)	Spatial and temporal T_{mrt}	Future climate scenarios
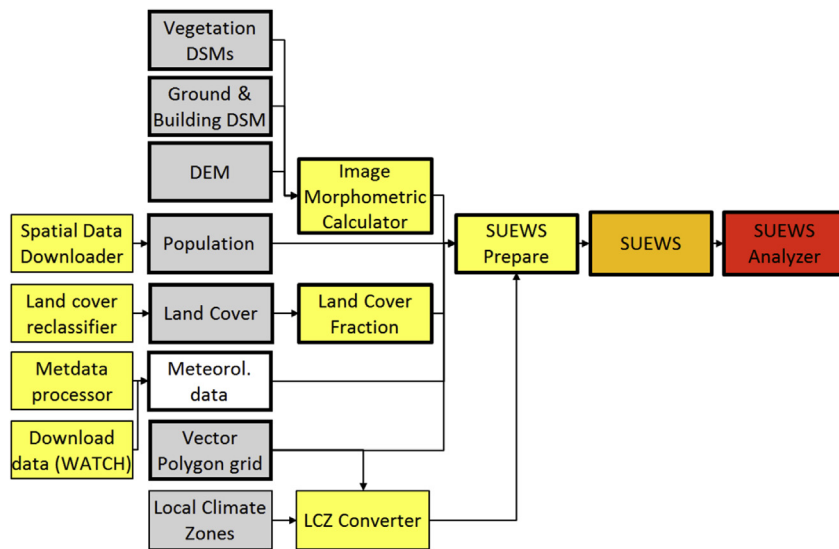
Fig. 3. Workflow and geodata for analysing urban energy balance using the SUEWS model. Bold outlined boxes are mandatory items. In some cases alternatives are shown. Yellow, orange and red indicates pre-processor, processor and post-processor tools, respectively (consistent with Fig. 1). Grey boxes indicate geodatasets and white boxes other types of data. DEM – digital elevation model, DSM – digital surface model, LCZ – local climate zones. It is strongly recommended that all geodata used are transformed into the same projected coordinate system. Model areas need to be defined in a vector polygon layer. For the meteorological forcing, users could manipulate their own data (**Metdata Processor**), use the WATCH – WFDEI climatological data set (**Download data (WATCH)**) or link to their own already-prepared data. (For interpretation of the references to colour in this figure legend, the reader is referred to the web version of this article.)
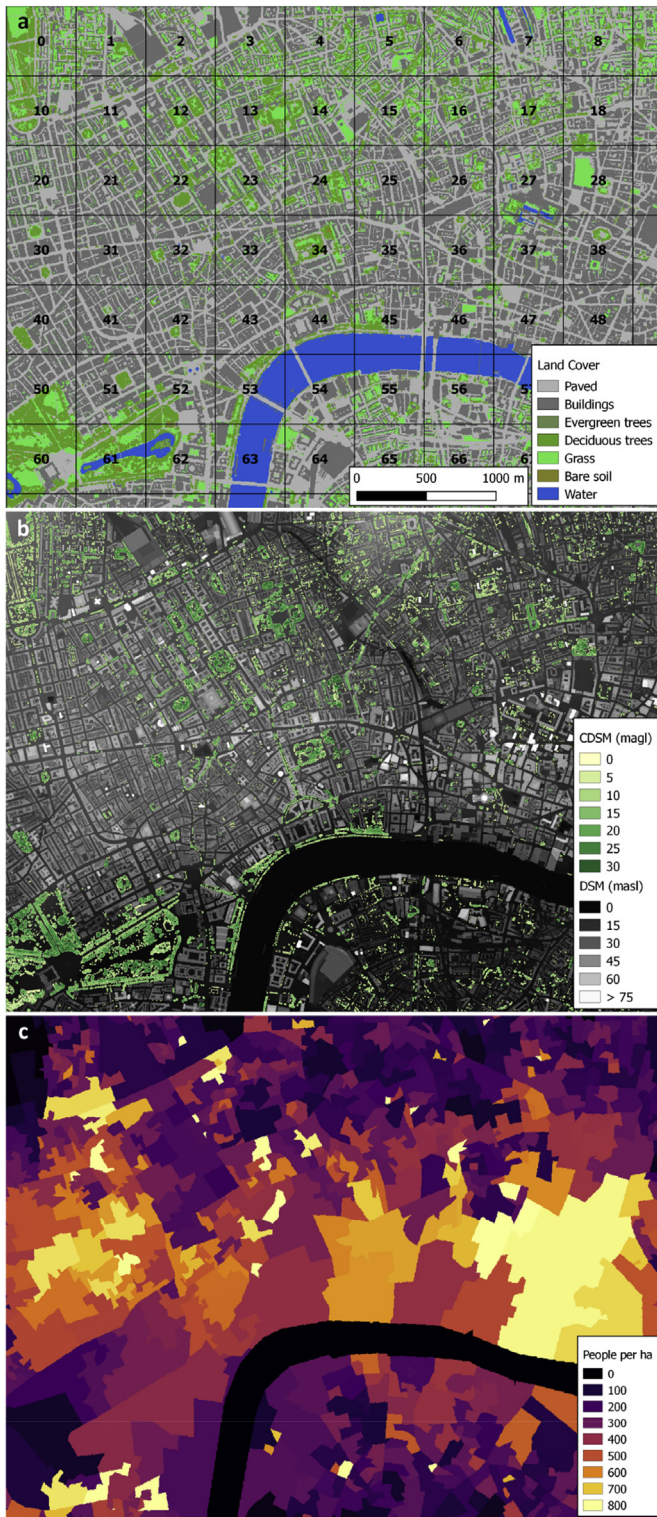
Fig. 4. Examples of input spatial data required to apply SUEWS for central London: **(a)** land cover overlain with a polygon grid for (dis-) aggregation (square grid created in QGIS, using Vector - > Research Tools - > Vector grid), **(b)** digital surface models (DSM) and canopy digital surface mode (CDSM) derived from an airborne LiDAR dataset obtained in the summers of 2005 and 2008 (Martin Holt, Infoterra Ltd., personal communication in 2011) and (**c**) population density (ONS, 2011). Population information can be (dis-)aggregated based on the polygon grid, through QGIS tool **Zonal Statistics**.

Fig. 7 shows the UMEP workflow to examine 3D radiant fluxes and T_{mrt}. Of the four geodatasets needed, the ground and building DSM (Fig. 8a) is fundamental. If available, a vegetation DSM (CDSM) can be added (Lindberg and Grimmond, 2011b). However, as 3D information on vegetation is sparse, the **Tree Generator** tool allows point vector data of tree locations to be transformed into a CDSM. Ground cover information can be used to estimate outgoing short and longwave radiation fluxes (Lindberg et al., 2016a,b). To obtain the appropriate ground cover classes, the **Land Cover Reclassifier** (Fig. 7) can be used to obtain the five ground cover classes (water, buildings, grass, paved and bare soil) used in **SOLWEIG** (Fig. 8b; no bare soil present).

The sky view factor (SVF) is the ratio between the radiation received (or emitted) by a planar surface and the radiation emitted (or received) by the entire hemispheric environment (Watson and Johnson, 1987). This dimensionless metric (totally obstructed = 0, totally unobstructed = 1) is important to human comfort (Fig. 8c), solar energy and solar access. A pixel-wise sky view factor calculated in **SVF** uses ground and building DSMs and/or vegetation DSM (Fig. 8c).

Solar access and radiative exchanges are impacted by wall height and aspect. **Wall height and aspect** (Tables 1 and 4, Fig. 7) provides wall pixels, with their height (Fig. 8d) and aspect (degrees). The latter is a modification of the Goodwin et al. (2009) linear filter (Lindberg et al., 2015b). To model T_{mrt} successfully, building footprint locations must be derived from either the ground cover grid or from differences between ground heights (DEM) and a DSM (Fig. 7).

SOLWEIG can be used for an individual time or a time series. For the latter, points of interest (POI) are added within the model domain. **SOLWEIG Analyzer** can be used to provide spatial (Fig. 8e) and temporal (Fig. 8f) visualizations of results. By comparing the input geodata (Fig. 8a–d) and the results (Fig. 8e–f), the micro-scale influences on the temporal and spatial patterns can be identified and explained. As shown in Fig. 8f, the temporal influence of T_{mrt} is unlike air temperature; it is highly affected by other variables, such as shortwave and longwave radiation fluxes.

Application of **SOLWEIG** to explore variations in T_{mrt} around the Civic Square (Medborgarplatsen) of central Stockholm shows that at 2 p.m., shadows from buildings and vegetation are important (Fig. 9). The highest T_{mrt} values are next to sunlit walls and on the sunlit open spaces. Open areas have high values T_{mrt} due to partly-cloudy conditions, which increases the proportion of diffuse shortwave radiation. The high values of T_{mrt} adjacent to the walls are related to the emitted longwave radiation and reflected short-wave radiation from the sunlit walls.

To explore the potential impact of T_{mrt}, it is useful to consider critical health thresholds. From analysis of Stockholm County daily all-cause mortality data (1990–2002), Thorsson et al. (2014) found that when T_{mrt} exceeds 59.4 °C there is an increase in heat-related mortality of 10% for those > 80 years of age. Using this threshold the areas of greatest hazard can be identified (adjacent to the sunlit buildings, Fig. 9b).

To determine the effects of warmer air temperature (+2 °C, +4 °C) the hazard can be re-analysed with further **SOLWEIG** simulations (Fig. 9c and d). The hazard increases in both areal and temporal extent with both open spaces and areas adjacent to sunlit walls being identified (cf. Fig. 9b). Walls have greater influence as air temperatures become warmer, as surface temperature of walls increase and emit more longwave radiation while the shortwave radiation in open spaces remains constant.
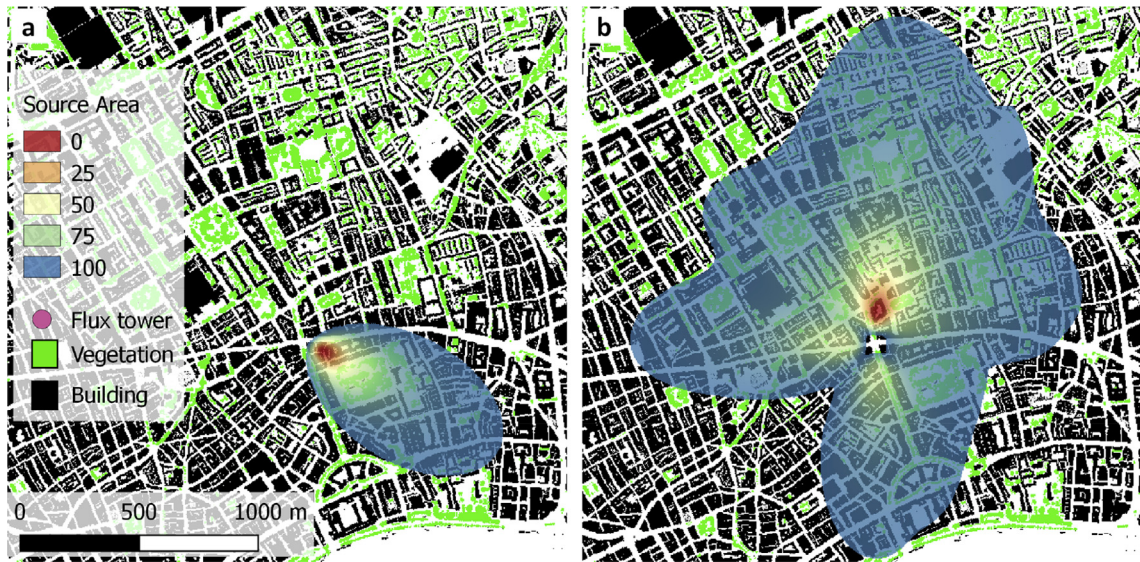
Fig. 5. The UMEP **Source Area Model** tool calculating the source area for: (a) individual meteorological conditions and (b) varying conditions to generate a source area climatology. Required input information includes a measurement location (x, y and z), a surface elevation database and meteorological conditions.
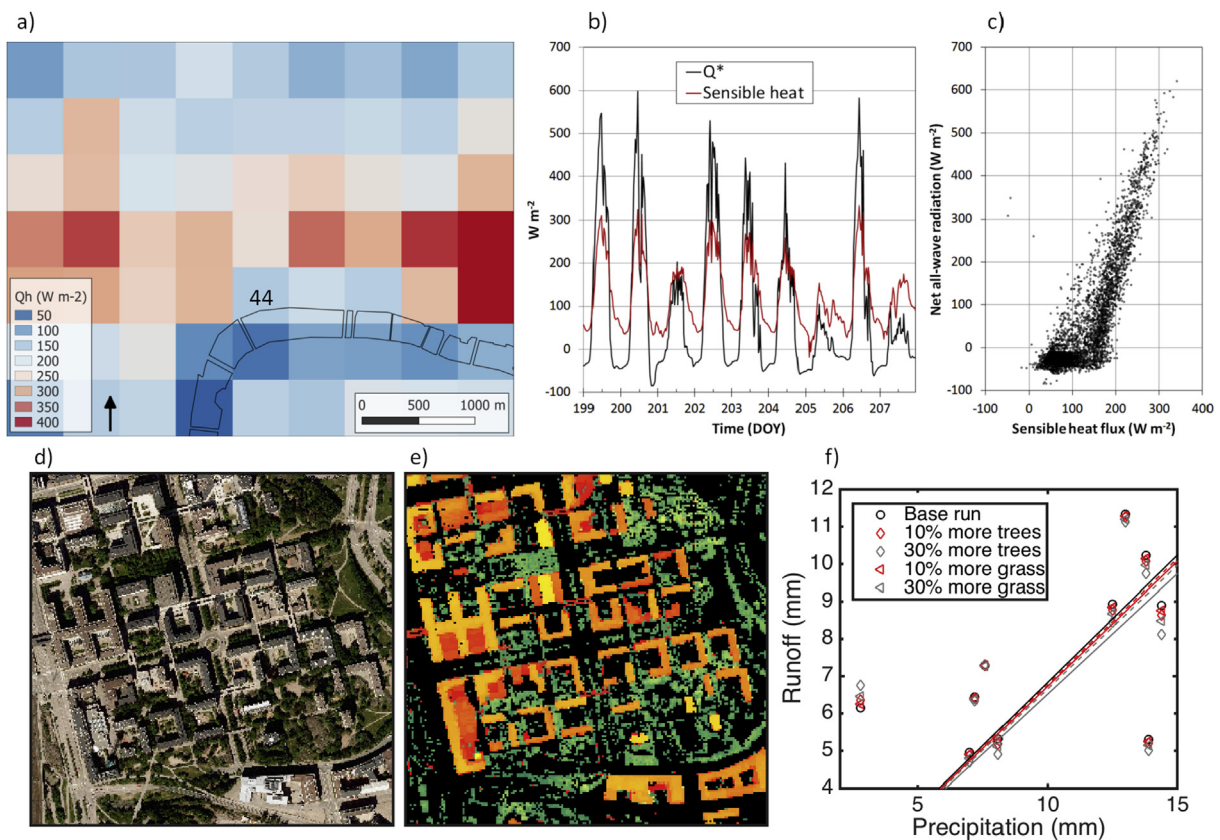

Fig. 6. Results from applications of **SUEWS** in (a–c) London, UK, 17 Jul - 27 Oct 2015 and (d–f) Helsinki September–November 2010. Examples of output from **SUEWS Analyzer**: (a) Average daytime sensible heat flux (Q_H), (b) time series of net radiation (Q^*) and Q_H for grid ID 44, (c) scatterplot between hourly values of Q^* and Q_H grid ID 44. (d) Aerial image of the water monitoring area (©2011 Kaupunkimittausosasto, Helsinki, Finland), (e) LiDAR derived land cover fractions (Nordbo et al., 2015), and (f) scatterplot between surface runoff and precipitation for different planning scenarios. Base run is the current case and in the alternative scenarios paved surfaces have been changed to street trees and grass areas. For visualisation, only events with runoff >4 mm have been plotted.
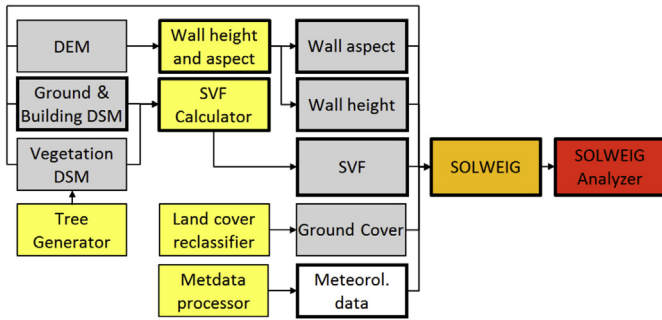
Fig. 7. Workflow and geodata used for analysing mean radiant temperature using SOLWEIG in UMEP. Bold outlines indicate mandatory items. Colour coding as in Fig. 3. (For interpretation of the references to colour in this figure legend, the reader is referred to the web version of this article.)

To investigate patterns at the city scale, the influence of building and vegetation density on T_{mrt} across Stockholm is examined at a pixel resolution of 1 m. The density of buildings and T_{mrt} show no strong correlation. However, there is a clear relation between T_{mrt} at 2 p.m. and vegetation density at the 500 m scale (Fig. 10). This demonstrates that increasing vegetation in urban areas could reduce T_{mrt} and mitigate heat stress.

3.4. Application example 4- Solar Energy on Building Envelopes

The contrast between sunlit and shaded surfaces can explain micro-scale differences in urban climate, for example spatial variation in road surface temperatures (Hu et al., 2015). In UMEP, sunlit fractions are computed using high resolution DSMs and the ShadowCalculator. The shadow casting algorithm uses sequential
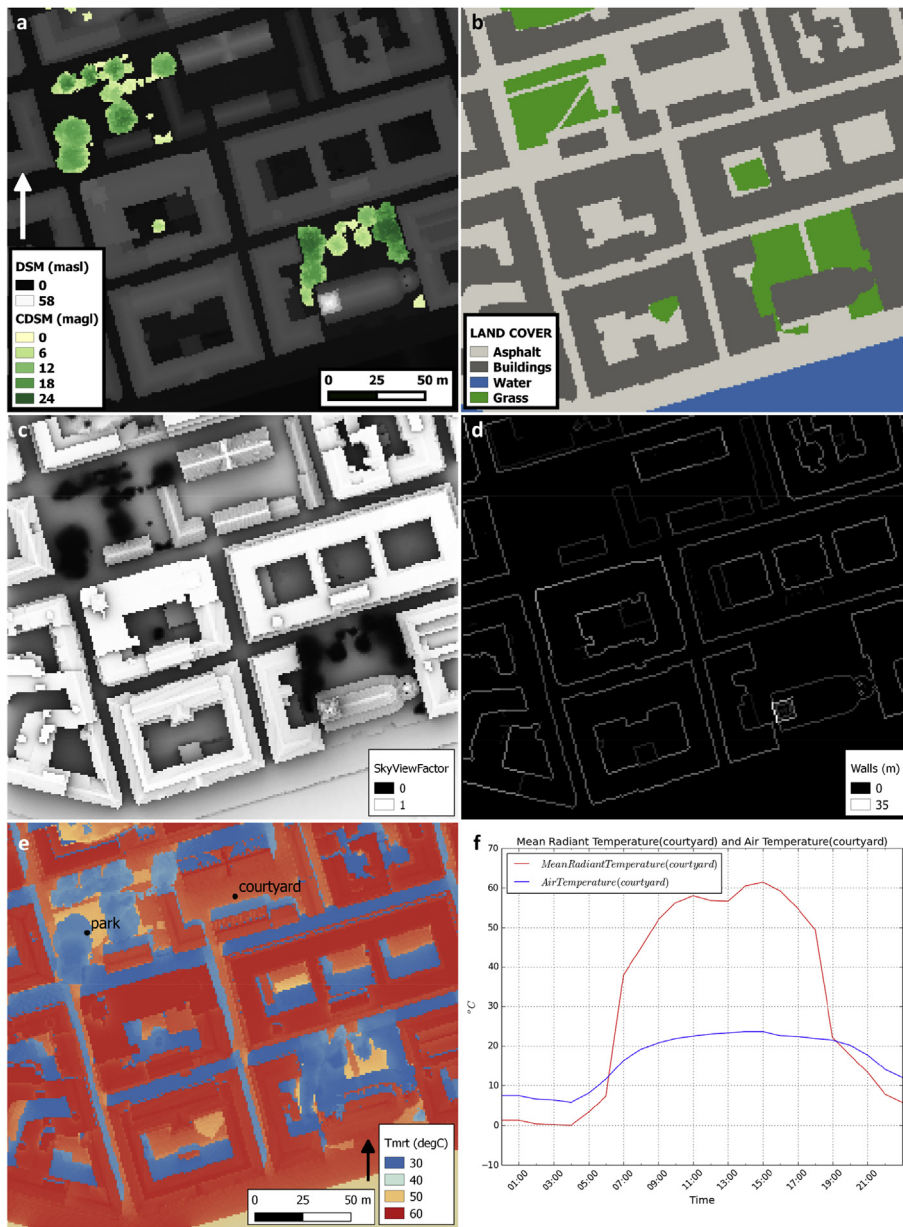

Fig. 8. SOLWEIG (a–d) spatial input and (e–f) output data displayed with **SOLWEIG Analyzer**. Inputs include "raw" data (a) digital surface models (DSM and CDSM), (b) ground cover, and UMEP derived data (see text) (c) sky view factor from buildings and vegetation, (d) wall pixels and height. The pixel resolution here is 1 m. T_{mrt} (°C) results for 26 July 2006 Gothenburg: (e) at 1 p.m., and (f) hourly T_{mrt} and air temperature (°C) for the courtyard point of interest (POI). The POI can be represented in any GDAL/OGR (a computer software library for reading and writing raster and vector geospatial data formats) point vector layer.
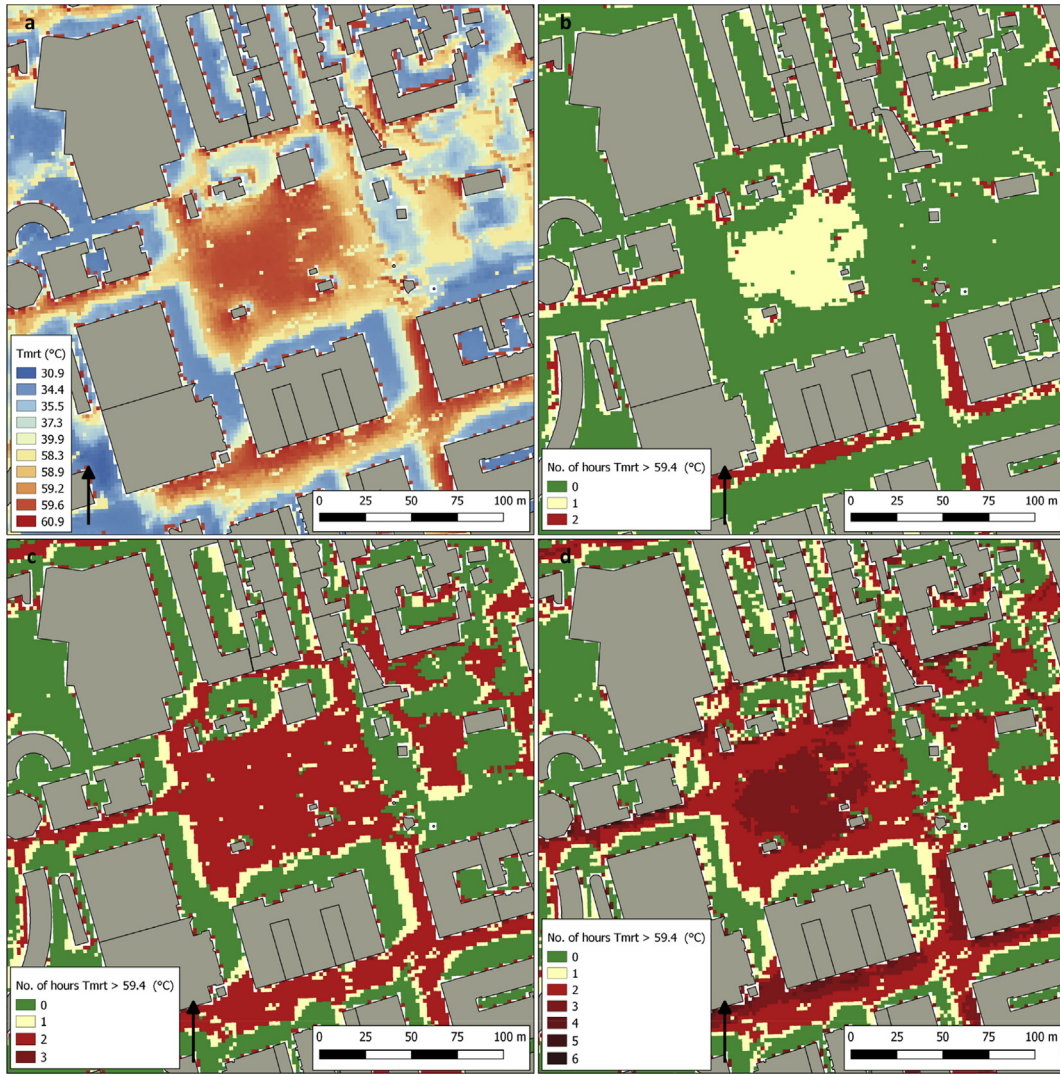
Fig. 9. The Civic Square (Medborgarplatsen) in Stockholm, Sweden (a) mean radiant temperature (T_{mrt}) at 14:00 using meteorological forcing from a hot summer day (28 July 1994) and (b) hazard map based on number of hours when $T_{mrt} > 59.4\ °C$ on one day, (c) same as (b) but with a 2 °C and (d) 4 °C increase in air temperature.

computation of 'shadow volumes' (Ratti and Richens, 1999) with a raster DSM (Ratti and Richens, 2004; Lindberg and Grimmond, 2010).

To map potential solar energy production, **SEBE** (Solar Energy on Building Envelopes) can calculate irradiances at pixel resolution on building roofs and walls using a 2.5-dimensional model. Observed solar radiation data are used with high resolution DSMs to derive accurate irradiances for the surfaces modelled (Lindberg et al., 2015a,b).

SEBE has been applied to several cities in Sweden (http://www.urban-climate.net/umep/Example_Applications). Fig. 11 shows a snapshot of an online mapping service where irradiance on roofs in Uppsala (14 km²) has been modelled in UMEP at 0.25 m resolution. The surface data are a combination of airborne LiDAR data and 3D vector polygons representing roof structures. For each building, post-processing analysis derived several statistics including areal extent (m²) of roofs and walls suitable for solar energy production (Fig. 11a) and the 3D distribution of solar irradiance (Fig. 11b).

3.5. Application example 5 − anthropogenic heat fluxes

Anthropogenic heat flux (Q_F), heat released directly by humans and their activities (Sailor, 2011), is a distinct feature of urban
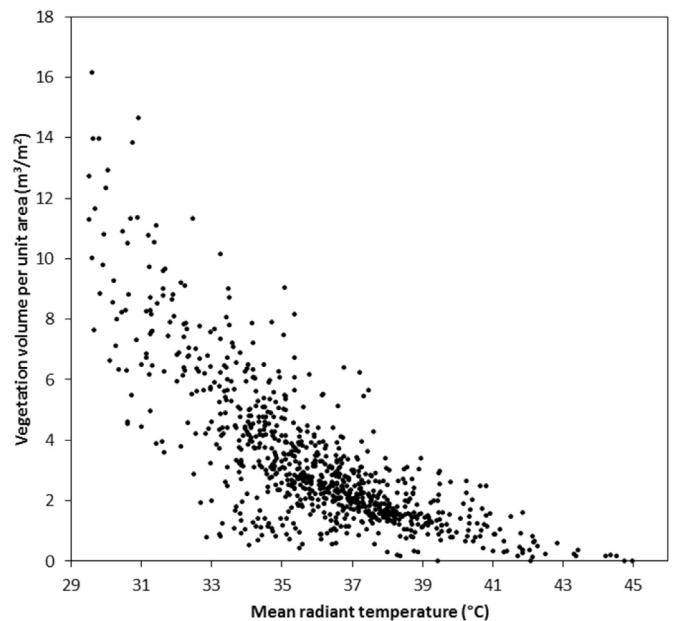

Fig. 10. SOLWEIG output showing the relation between average ground surface T_{mrt} and vegetation volume for 500 m × 500 m grids in Stockholm, Sweden on the 28 July at 2 p.m.

Fig. 11. **SEBE** results for an online application for rooftop irradiance in central Uppsala, Sweden, (a) pop-up window with statistics for one of the buildings, (b) 3D view of shortwave irradiance (walls and roof) for the building. (www.uppsala.se/solkarta) Meteorological data used in this example originate from a meso-scale model for solar radiation (STRÅNG, www.strang.smhi.se) developed by the Swedish Meteorological and Hydrological Institute (SMHI).

areas with significant impact on energy and water exchanges. In UMEP, in addition to the methods within SUEWS, Q_F can be modelled using two standalone approaches (Appendix 2): (i) **LQF**, which uses the LUCY methodology (Allen et al., 2011; Lindberg et al., 2013a) and provides simple estimates at low spatial resolution; and (ii) **GQF**, which is a reimplementation of GreaterQF (Iamarino et al., 2012), and produces high-resolution estimates with greater insights into specific types of energy use. In UMEP, each has been supplemented with a spatial input data preprocessor that makes use of standard GIS data formats, and outputs spatially and temporally-resolved Q_F estimates of traffic ($Q_{F,T}$), metabolic ($Q_{F,M}$) and building ($Q_{F,B}$) emissions in Universal Coordinated Time. The LQF results can be incorporated into the meteorological data used to force SUEWS via the refinement stage of the **Download data (WATCH)** tool.

An example of **LQF** output across Greater London in October 2015 using Local Super Output Area (LSOA) population data shows the spatial distribution of each component, and the resultant larger Q_F towards the city centre (Fig. 12b, d, f). The assumptions applied here limit **LQF** to spatial scales of the order 1 km (Gabey et al., 2017). At spatial scales less than 1 km, movements of people, for example from home to work, are important and the structure of the road network needs to be captured (Gabey et al., 2017). Example output maps from **GQF** (Fig. 12a, c, e) show order-of-magnitude agreement with **LQF**, with a notably different spatial structure in $Q_{F,T}$ (Fig. 12c, d) because road network topology is used rather than population count. The effect of using the workday (**GQF**) rather than residential (**LQF**) population on the daytime metabolic emission (Fig. 12e, f) is visible as a strong enhancement in the centre of the city. A similar enhancement is also evident in the building emissions (Fig. 12 a, b), which is attributable to the use of spatially-resolved energy consumption in **GQF** compared with residential population-based attribution in **LQF**.
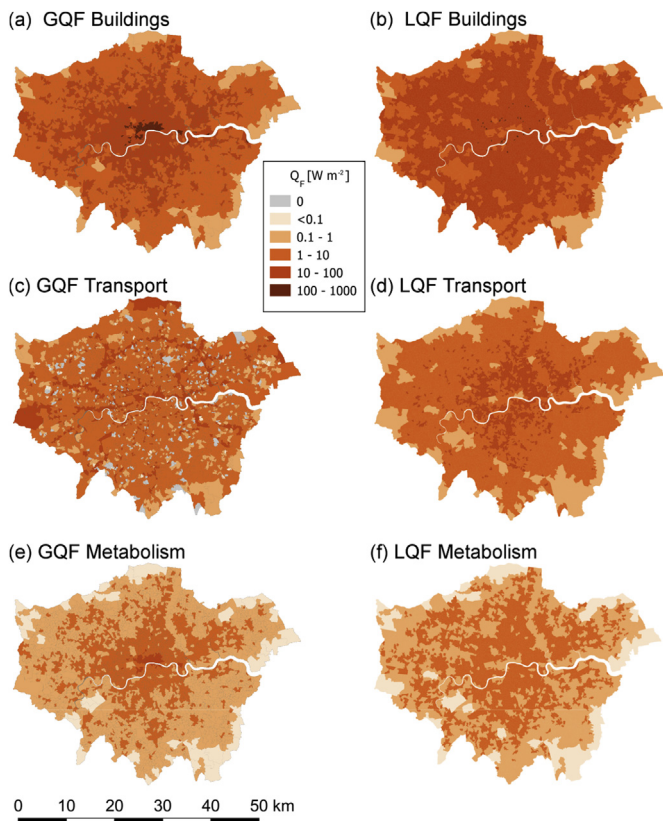
Fig. 12. Example outputs from (left) **GQF** and (right) **LQF** Greater London on 2nd October 2015 at 11:00 UTC. (a,b) Building, (c,d) transport and (e,f) metabolic emissions are shown to highlight the different spatial distributions that the models produce. The same colour scale is used for all maps. Appendix 2 provides more details about the two methods.

4. Concluding comments

The city based climate service tool UMEP (Urban Multi-scale Environmental Predictor) is introduced through a series of applications. The QGIS plug-in has a coupled modelling system of "state of the art" 1-D and 2-D models which can provide estimates of essential urban climate processes. It also provides tools for determining parameters for more complex 3-D models. A key contribution of UMEP is to provide a method to consistently determine model parameters across a suite of models and applications. This serves to ensure consistency in theoretical assumptions between models, data analysis, observations, evaluation and applications (different scales, applications and end users). Common processing tools also enable rapid updates when new data become available (for example, release of new national statistical data used in the anthropogenic heat flux) or when new parameterisations are developed (for example, new aerodynamic roughness models of Kent et al., 2017a,b) which can then be used to understand flux measurements (**Source Area Model**) and to perform energy and water balance calculations (**SUEWS**).

Example applications have been presented to illustrate UMEP's potential, specifically of the identification of heat waves and cold waves in cities (**ExtremeFinder**); the implications of green infrastructure on runoff (**SUEWS**); micro-scale heat stress (**SOLWEIG**); solar energy production (**SEBE**); and sources of anthropogenic (human-generated) heat (**LQF**, **GQF**). Each application draws on different combinations of UMEP tools.

UMEP is under active development and refinement. It is designed as an open source tool, the development team welcomes all kinds of collaboration through, for example, submission of comments or issues to the repository (www.bitbucket/fredrik_ucg/umep/), participation in coding, addition of new features and development of new tutorials for users. The online manual provides more details on how to participate (http://www.urban-climate.net/umep/UMEP_Manual). Planned developments include tools for pedestrian wind and thermal comfort indices.

Software availability

Name of software: Urban Multi-scale Environmental Predictor (UMEP)
Developers: Fredrik Lindberg, Sue Grimmond, Andrew Gabey, Bei Huang, Christoph W Kent, Ting Sun, Natalie E Theeuwes, Isabella Capel-Timms, Leena Järvi, Helen C Ward, Yuanyong Chang, Niklas Krave, D Meyer, Frans Olofson, Jianguo Tan, Dag Wästberg, Lingbo Xue, Zhe Zhang
Contact: Fredrik Lindberg: fredrikl@gvc.gu.se, +46 31 786 2606 Sue Grimmond: c.s.grimmond@reading.ac. +44 118 378 6248
Year first available: 2015
Hardware required: NA
Software required: QGIS 2.X
Operation system required: OS independent
Program language: Python
Program size: ~2.5 Mb (compressed), ~9 Mb (uncompressed)
Availability and cost: Open source (no cost)
Repository: www.bitbucket.org/fredrik_ucg/umep
Webpage: www.urban-climate.net/umep

Appendix 1. Meteorological information

UMEP uses a common data format for meteorological data (Table A1.1). Preparing Existing Data (Figure A1.1), imports variables from ASCII files and allows for time related variables (year, day of year, hour and minute) and other time formats (such as month, day of month etc.) in preparation for analysis. During this process, some quality control is performed to ensure the data are within reasonable limits (Table A1.1, Figure A1.1) and to identify missing time intervals.
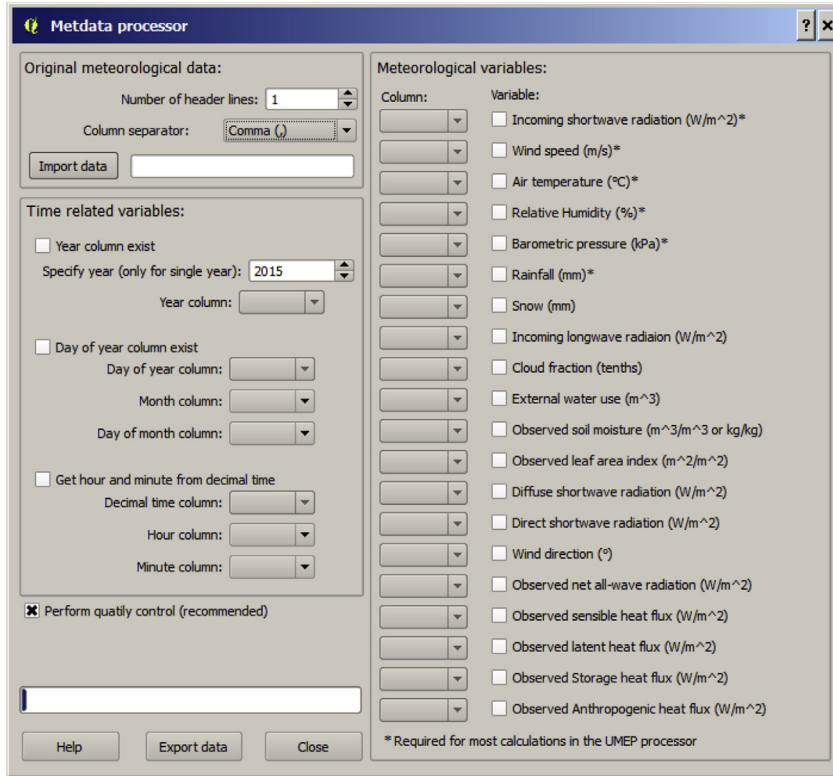
Fig. A1.1. Example dialogue box in UMEP - **Meteorological processor**.

Download data (WATCH) provides another source of meteorological forcing data (section 3.1), global reanalysis products, if observed data are not available. However, the coarse spatial resolution of reanalysis products (e.g. grids of 0.5°) means that downscaling is needed prior to their use for local-scale urban hydrological modelling (Wilby et al., 2000; Fowler et al., 2007; Bastola and Misra, 2014). The methods used to prepare the data are based on Best and Grimmond (2016), Kokkonen et al. (2017) and Ward et al. (2017a). These involve:

(i) Identification of the area of interest, (ii) download of the data, and (iii) generation of a UMEP-formatted file with data aligned to the appropriate time zone at hourly intervals.

These UMEP WFDEI data corrections are dependent on the meteorological variables, as some are instantaneous values whereas others are averages for a 3-h period (Weedon et al., 2011, Ward et al., 2017a). The 3-h data are linearly interpolated to 1-h

data. However, for the incoming solar radiation the times of sunrise and sunset are calculated to ensure that the day length is as expected and the interpolated data are adjusted to take this into account. For instance, if sunrise and sunset times are 6:00 LT (local time) and 19:00 LT, respectively, only the interpolated values between 6:00 LT and 19:00 LT will have non-zero short wave radiation, but are rescaled for that period retaining the daily average.

The relative humidity (RH) is obtained from the specific humidity (q_v, in kg kg-1) as follows: $RH = \frac{e_a}{e_s} \times 100$

With e_a and e_s the actual and saturation vapor pressures (Buck, 1981) given by

$$e_a = \frac{R_V q_v p}{R_d + q_v (R_v - R_d)}$$

$$e_s = \begin{cases} 6.1121 \exp\left(\dfrac{\left(18.678 - \dfrac{T_C}{234.5}\right) T_C}{T_C + 257.14}\right)\left(1.00072 + p\left(3.2 \times 10^{-6} + 5.9 \times 10^{-10} T_C^2\right)\right) & T_C \geq 0\,°C \\[30pt] 6.1115 \exp\left(\dfrac{\left(23.036 + \dfrac{T_C}{333.7}\right) T_C}{T_C + 279.82}\right)\left(1.00022 + p\left(3.83 \times 10^{-6} + 6.4 \times 10^{-10} T_C^2\right)\right) & T_C < 0\,°C \end{cases}$$

where $R_v = 461.5$ J K^{-1} kg^{-1} the specific gas constant for water vapour, $R_d = 287.04$ J K^{-1} kg^{-1} the specific gas constant for dry air, p the atmospheric pressure (kPa) and T_C the air temperature (°C).

Other corrections consider the effect of elevation. With a coarse grid the city or of area of interest may be at a lower elevation than the surroundings. As one example, Vancouver, the real weighted mean WFDEI grid height includes mountains but much of the city is much lower (Kokkonen et al., 2017). Thus, consideration needs to be given to: (i) the elevation of the area of interest, (ii) the height of the roughness elements (buildings, trees), and (iii) the appropriate height for the forcing data for the simulation. In UMEP, the WFDEI temperature and pressure values are adjusted to the simulation height using environmental lapse rate ($\Gamma = -6.5$ °C km^{-1}) and the hypsometric equation (Weedon et al. 2011). RH, used by SUEWS, is calculated from the WFDEI specific humidity assuming it is constant with altitude to avoid supersaturation. Interpolation and altitude corrections may require a spin-up period to avoid interpolation errors and missing data points at the beginning and at the end of the time series. Thus, longer periods should be used for analysis than the period of specific interest.

Appendix 2. Anthropogenic heat flux

LQF is designed to provide "out-of-the-box" anthropogenic heat flux (Q_F) estimates at 1-h time steps. The minimum user-provided input data required are the spatially-resolved population count and a daily mean air temperature time series. Both data sets can be obtained using tools within UMEP. Heat fluxes are estimated using a top-down methodology that draws on a database of national energy consumption, population and vehicle ownership statistics. **LQF** attributes this energy consumption and traffic based on local population count variations, and estimates Q_F in each population area. It is possible to replace the national data with provincial or smaller regions if the data are available.

The database contains diurnal variations for metabolism, traffic flow and building energy consumption, which are optionally overridden with user-specified versions. Weekend/weekday variations are captured for buildings ($Q_{F,B}$) and transport ($Q_{F,T}$), while the user-specified versions provide control over each day of the week. Day-to-day building energy consumption is estimated using a database-held, country-specific temperature response function and assumption about the prevalence of air-conditioning (Lindberg et al., 2013a). A blanket weekend traffic reduction is also applied to capture day-of-week traffic flow changes.

Table A1.1

Meteorological data used in various components of UMEP are formatted in the order indicated. The **Metdata Pre-processor** tool does simple quality control to ensure data are within acceptable ranges. Not all variables are required in UMEP (with the exception of the four time-related columns): All − any that use meteorological data, SU − **SUEWS**, SO − **SOLWEIG**, SA − source area model, SE − **SEBE**, for some application these data are required (**Bold**). The variables extracted by **Download data (WATCH)** are indicated (column 5). When data are not needed it can be assigned −999 to indicate no data available. Day of year is used instead of date within a month for simplicity. The hour and minute is local standard time and refers to time ending.

No.	Description (units)	Accepted range	Used by	WATCH
1	Year [YYYY]		All	
2	Day of year [DOY]		All	
3	Hour [H]		All	
4	Minute [M]		All	
5	Net all-wave radiation [W m^{-2}]	−200 to 800	SU	
6	Sensible heat flux [W m^{-2}]	−200 to 750	SU	
7	Latent heat flux [W m^{-2}]	−100 to 650	SU	
8	Storage heat flux [W m^{-2}]	−200 to 650	SU	
9	Anthropogenic heat flux [W m^{-2}]	0 to 1500	SU	
10	Wind speed [m s^{-1}]	0.001 to 60	**SU**/SA	X
11	Relative Humidity [%]	5 to 100	**SU**/**SO**/SE	X
12	Air temperature [°C]	−30 to 55	**SU**/**SO**/SE	X
13	Barometric pressure [kPa]	90 to 107	**SU**/**SO**	X
14	Rainfall [mm]	0 to 30 (per 5 min)	**SU**	X
15	Incoming shortwave radiation [W m^{-2}]	0 to 1200	**SU**/**SO**/**SE**	X
16	Snow [mm]	0 to 300 (per 5 min)	SU	X
17	Incoming longwave radiation [W m^{-2}]	100 to 600	SU	X
18	Cloud fraction [tenths]	0 to 1	SU	
19	External water use [m^3]	0 to 10 (per 5 min)	SU	
20	Observed soil moisture [m^3 m^{-3} or kg kg^{-1}]	0.01 to 0.5	SU	
21	Observed leaf area index [m^2 m^{-2}]	0 to 15	SU	
22	Diffuse shortwave radiation [W m^{-2}]	0 to 600	SO/SE	
23	Direct shortwave radiation [W m^{-2}]	0 to 1200	SO/SE	
24	Wind direction [°]	0 to 360	SU/SA	
25	Friction velocity [m s^{-1}]	All	SA	
26	Standard Deviation (sigma) of transverse-wind velocity [m s^{-1}]	All	SA	
27	Obukhov Length [m]	All	SA	
28	Boundary layer height [m]	All	SA	

Table A2.1

Input data files required by the LQF model

Dataset	Type	Remarks
Population count	Polygon shapefile	Basis of spatial variations of Q_F components
Daily mean temperature	CSV file(s)	Basis of day-to-day building energy consumption variations
Traffic diurnal profile	CSV file(s)	Optional
Building energy diurnal profile	CSV file(s)	Optional
LQF database	Spatialite file	Downloaded from UMEP website; can be edited by user

GQF produces Q_F estimates at higher spatial resolution and 30-min time steps, but requires comprehensive input data (Table A2.2) to support this. The shift in population distribution during working days is captured using residential and workday population datasets, with morning and evening transition periods. Road transport emissions are calculated using a vector map containing every road link, along with the road class label and traffic flow broken down by vehicle type. Maps of residential and non-residential gas and electricity consumption across the city are used to estimate building emissions. The model therefore sub-divides $Q_{F,T}$ by vehicle type, and $Q_{F,B}$ by fuel and consumer, and estimates the spatial distribution of transport emissions independently of the population distribution. Model spatial resolution is dictated by the input residential and workday population datasets, with the annual energy consumption data disaggregated to common spatial units based on population.

Day-to-day variations in building energy consumption and hence $Q_{F,B}$ are captured using empirical demand data from utility companies, and half-hourly variations are obtained from week-long diurnal profiles, with separate profiles specified for each energy consumption category. Temporal variations in transport are governed by a week-long diurnal profile for each vehicle type, in which some days have greater mean values than others to reflect day-to-day traffic variations. This segmentation means the temporal evolution of each Q_F component in a modelled area depends on the balance of vehicle types, energy consumers and the residential to workday population ratio. **GQF** also partitions $Q_{F,T}$, $Q_{F,B}$ and metabolism ($Q_{F,M}$) into sensible, latent and (for buildings) wastewater fractions. These can be included or excluded from the modelled Q_F at model run time.

Table A2.2
Input data sources required by the **GQF** model.

Data source	Type	Remarks
Residential population count	Polygon shapefile	Used for metabolism estimates and to spatially disaggregate energy consumption data to common spatial units.
Workday population count	Polygon shapefile	
Road network and traffic flow	Line shapefile	Each road segment with road classification and annual average daily total traffic for each vehicle type
Residential energy consumption:	Shapefiles	Spatially disaggregated using residential population
Residential electricity		
Residential gas		
Residential economy 7		
Non-residential energy consumption:	Shapefiles	kWh per year, spatially-resolved within city Spatially disaggregated using workday population
Non-residential electricity		
Non-residential gas		
Non-residential other		
Daily energy consumption time series	CSV file	Relative variations used to scale annual to daily values. Applied to both residential and non-residential sectors.
Gas		
Electricity		
Vehicle diurnal profiles	CSV file	Time series for each vehicle type
Building energy diurnal profiles	CSV file	Time series for energy consumption dataset
Metabolic diurnal profiles	CSV file	Time series defining metabolic rate per person and transition between workday and residential population.
Vehicle fuel efficiencies	CSV file	Amount of fuel consumed per vehicle class and fuel type

References

Alcoforado, M.J., Andrade, H., Lopes, A., Vasconcelos, J., 2009. Application of climatic guidelines to urban planning: the example of Lisbon (Portugal). Landsc. Urban Plan. 90 (1—2), 56—65.

Alexander, P.J., Mills, G., Fealy, R., 2015. Using LCZ data to run an urban energy balance model. Urban Clim. 13, 14—37.

Alexander, P.J., Bechtel, B., Chow, W.T.L., Fealy, R., Mills, G., 2016a. Linking urban climate classification with an urban energy and water budget model: Multi-site and multi-seasonal evaluation. Urban Clim. 17, 196—215.

Alexander, P.J., Fealy, R., Mills, G., 2016b. Simulating the impact of different urban development pathways on the local climate: a scenario-based analysis in the greater Dublin region, Ireland. Landsc. Urban Plan. 152, 72—89.

Allen, L., Lindberg, F., Grimmond, C.S.B., 2011. Global to city scale urban anthropogenic heat flux: model and variability. Int. J. Climatol. 31 (13), 1990—2005.

Ao, X., Grimmond, C.S.B., Chang, Y., Liu, D., Tang, Y., Hu, P., Wang, Y., Zou, J., Tan, J., 2016. Heat, water and carbon exchanges in the tall megacity of Shanghai: challenges and results. Int. J. Climatol. 36 (14), 4608—4624.

Baklanov, A., Grimmond, C.S.B., Carlson, D., Terblanche, D., Tang, X., Bouchet, V., Lee, B., Langendijk, G., Kolli, R.K., Hovsepyan, A., 2017. From urban meteorology, climate and environment research to integrated city services. Urban Clim. https://doi.org/10.1016/j.uclim.2017.05.004.

Bastola, S., Misra, V., 2014. Evaluation of dynamically downscaled reanalysis precipitation data for hydrological application. Hydrol. Process. 28, 1989—2002. https://doi.org/10.1002/hyp.9734.

Best, M.J., Grimmond, C.S.B., 2016. Modelling the Bowen ratio at a number of urban sites over a range of vegetation cover. J. Hydrometeorol. http://journals.ametsoc.org/doi/10.1175/JHM-D-15-0126.1.

Best, M.J., Pryor, M., Clark, D.B., Rooney, G.G., Essery, R.L.H., Ménard, C.B., Edwards, J.M., Hendry, M.A., Porson, A., Gedney, N., Mercado, L.M., Sitch, S., Blyth, E., Boucher, O., Cox, P.M., Grimmond, C.S.B., Harding, R.J., 2011. The joint UK land environment simulator (JULES), model description — Part 1: energy and water fluxes. Geosci. Model Dev. 4, 677—699.

Bottema, M., Mestayer, P.G., 1998. Urban roughness mapping—validation techniques and some first results. J. Wind Eng. Ind. Aerodyn. 74, 163—173.

Bruse, M., Fleer, H., 1998. Simulating surface-plant-air interactions inside urban environments with a three dimensional numerical model. Environ. Model. Softw. 13 (3—4), 373—384.

Buck, A.L., 1981. New equations for computing vapor pressure and enhancement factor. J. Appl. Meteorol. 20 (12), 1527—1532.

Busuioc, A., Caian, M., Cheval, S., Bojariu, R., Boroneanţ, C., Baciu, M., Dumitrescu, Al, 2010. Variabilitatea Şi Schimbarea Climei În România, Edit. ProUniversitaria, Bucureşti, p. 226 (cited by Micu 2012).

Chen, L., Yu, B., Yang, F., Mayer, H., 2016. Intra-urban differences of mean radiant temperature in different urban settings in Shanghai and implications for heat stress under heat waves: a GIS-based approach. Energy Build. 130, 829—842.

Ching, J., Mills, G., Bechtel, B., See, L., Feddema, J., Wang, X., Ren, C., Brousse, O., Martilli, A., Neophytou, M., Mouzourides, P., Stewart, I., Hanna, A., Ng, E., Foley, M., Alexander, P.J., Aliaga, D., Niyogi, D., Shreevastava, A., Bhalachandran, P., Masson, V., Hidalgo, J., Fung, J., Andrade, M., Baklanov, A., Dai, W., Milcinski, G., Demuzere, M., Brunsell, N., Pesaresi, M., Miao, S., Mu, Q., Chen, F., Theeuwes, N., 2017. World urban database and access portal tools (WUDAPT), an urban weather, climate and environmental modeling infrastructure for the anthropocene. Bull. Am. Meteorol. Soc. (under review).

Chrysoulakis, N., Lopes, M., San José, R., Grimmond, C.S.B., Jones, M.B., Magliulo, V., Klostermann, J.E.M., Synnefa, A., Mitraka, Z., Castro, E.A., González, A., Vogt, R., Vesala, T., Spano, D., Pigeon, G., Freer-Smith, P., Staszewski, T., Hodges, N., Mills, G., Cartalis, C., 2013. Sustainable urban metabolism as a link between biophysical sciences and urban planning: the BRIDGE project. Landsc. Urban Plan. 112, 100—117. https://doi.org/10.1016/j.landurbplan.2012.12.005.

Dee, D.P., Uppala, S.M., Simmons, A.J., Berrisford, P., Poli, P., Kobayashi, S., Andrae, U., Balmaseda, M.A., Balsamo, G., Bauer, P., Bechtold, P., Beljarrs, A.C.M., van de Berg, L., Bidlot, J., Bormann, N., Delsol, C., Dragani, R., Fuentes, M., Geer, A.J., Haimberger, L., Healy, S.B., Hersbach, H., Holm, E.V., Isaksen, L., Kallberg, P., Kohler, M., Matricardi, M., McNally, A.P., Monge-Sanz, B.M., Morcrette, J.-J., Park, B.-K., Peubey, C., de Rosnay, P., Tavolato, C., Thepaut, J.-N., Vitart, F., 2011. The ERA-Interim reanalysis: configuration and performance of the data assimilation system. Q. J. R. Meteorol. Soc. 137, 553—597.

Demuzere, M., Harshan, S., Järvi, L., Roth, M., Grimmond, C.S.B., Masson, V., 2017. Impact of urban canopy models and external parameters on the modelled urban energy balance in a tropical city. Q. J. R. Meteorol. Soc. https://doi.org/10.1002/qj.3028.

Dong, Y., Varquez, A.C.G., Kanda, M., 2017. Global anthropogenic heat flux database with high spatial resolution. Atmos. Environ. 150, 276—294. https://doi.org/10.1016/j.atmosenv.2016.11.040.

Dudhia, J., 2014. A history of mesoscale model Development. Asia-Pac. J. Atmos. Sci. 50, 121—131.

Eliasson, I., 2000. The use of climate knowledge in urban planning. Landsc. Urban Plan. 48, 31—44.

Fischer, E.M., Schär, C., 2010. Consistent geographical patterns of changes in high-impact European heatwaves. Nat. Geosci. 3 (6), 398—403.

Fowler, H.J., Blenkinsop, S., Tebaldi, C., 2007. Linking climate change modelling to impacts studies: recent advances in downscaling techniques for hydrological modelling. Int. J. Climatol. 27, 1547—1578. https://doi.org/10.1002/joc.1556.

Gabey, A., Grimmond, C.S.B., Capel-Timms, I., 2017. Anthropogenic Heat Flux: at what spatial resolution is a simple model reasonable? Theor. Appl. Climatol. (under review).

Goodwin, N.R., Coops, N.C., Tooke, T.R., Christen, A., Voogt, J.A., 2009. Characterizing urban surface cover and structure with airborne lidar technology. Can. J. Remote Sens. 35, 297–309.

Grimmond, C.S.B., 2013. Observing London: Weather Data Needed for London to Thrive, London Climate Change Partnership, p. 82. http://climatelondon.org.uk. London Climate Change Partnership, Lloyds, Met Office.

Grimmond, C.S.B., Oke, T.R., 1991. An evaporation-interception model for urban areas. Water Resour. Res. 27, 1739–1755.

Grimmond, C.S.B., Oke, T.R., 1999. Aerodynamic properties of urban areas derived from analysis of surface form. J. Appl. Meteorol. 38, 1262–1292.

Grimmond, C.S.B., Tang, X., Baklanov, A., 2014. Towards integrated urban weather, environment and climate services. WMO Bull. 63 (1), 10–14. https://googledrive.com/host/0BwdvoC9AeWjUazhkNTdXRXUzOEU/bulletin_63-1_en.pdf. http://library.wmo.int/opac/index.php?lvl=notice_display&id=15965.

Herbert, J.M., Johnson, G.T., Arnfield, A.J., 1998. Modelling the thermal climate in city canyons. Environ. Model. Softw. 13 (3), 267–277.

Horton, R., Rosenzweig, C., Solecki, W., Bader, D., Sohl, L., 2016. Climate science for decision-making in the New York metropolitan region. In: Parris, A.S., Garfin, G.M., Dow, K., Meyer, R., Close, S.L. (Eds.), Climate in Context: Science and Society Partnering for Adaptation. John Wiley & Sons, Ltd, Chichester, UK. https://doi.org/10.1002/9781118474785.ch3.

Hu, Y., Almkvist, E., Lindberg, F., Bogren, J., Gustavsson, T., 2015. The use of screening effects in modelling route-based daytime road surface temperature. Theor. Appl. Climatol. 125 (1), 303–319.

Iamarino, M., Beevers, S., Grimmond, C.S.B., 2012. High-resolution (space, time) anthropogenic heat emissions: London 1970–2025. Int. J. Climatol. 32 (11), 1754–1767.

Jänicke, B., Meier, F., Lindberg, F., Schubert, S., Scherer, D., 2016. Towards city-wide, building-resolving analysis of mean radiant temperature. Urban Clim. 15, 83–98.

Järvi, L., Grimmond, C.S.B., Christen, A., 2011. The surface urban energy and water balance scheme (SUEWS): evaluation in los angeles and vancouver. J. Hydrol. 411, 219–237.

Järvi, L., Grimmond, C.S.B., Taka, M., Nordbo, A., Setälä, H., Strachan, I.B., 2014. Development of the surface urban energy and water balance scheme (SUEWS) for cold climate cities. Geosci. Model Dev. 7, 1691–1711. https://doi.org/10.5194/gmd-7-1691-2014.

Järvi, L., Grimmond, C.S.B., McFadden, J.P., Christen, A., Strachan, I., Taka, M., Warsta, L., Heimann, M., 2017. Warming effects on the urban hydrology in cold climate regions. Sci. Rep. 7, 5833. https://doi.org/10.1038/s41598-017-05733-y.

Kanda, M., Inagaki, A., Miyamoto, T., Gryschka, M., Raasch, S., 2013. A new aerodynamic parametrization for real urban surfaces. Bound.-Layer Meteorol. 148, 357–377.

Karsisto, P., Fortelius, C., Demuzere, M., Grimmond, C.S.B., Oleson, K., Kouznetsov, R., Masson, V., Järvi, L., 2015. Seasonal surface urban energy balance and wintertime stability simulated using three land-surface models in the high-latitude city Helsinki. Q. J. R. Meteorol. Soc. 142 (694), 401–417. https://doi.org/10.1002/qj.2659.

Keevallik, S., Vint, K., 2015. Temperature extremes and detection of heat and cold waves at three sites in Estonia. Proc. of the Est. Acad. Sci vol. 64 (No. 4), 473–479.

Kent, C.W., Grimmond, C.S.B., Barlow, J., Gatey, D., Kotthaus, S., Lindberg, F., Halios, C.H., 2017a. Evaluation of urban local-scale aerodynamic parameters: implications for the vertical profile of wind speed and for source areas. Boundary-Layer Meteorol. 164, 183–213.

Kent, C.W., Grimmond, C.S.B., Gatey, D., 2017b. Aerodynamic roughness parameters in cities: inclusion of vegetation. J. Wind Eng. Industrial Aerodynamics 169, 168–176.

Kljun, N., Calanca, P., Rotach, M.W., Schmid, H.P., 2015. A simple two-dimensional parameterisation for Flux Footprint Prediction (FFP). Geosci. Model Dev. 8, 3695–3713. https://doi.org/10.5194/gmd-8-3695-2015, 2015.

Kokkonen, T., Grimmond, C.S.B., Räty, O., Ward, H.C., Christen, A., Oke, T., Kotthaus, S., Järvi, L., 2017. Sensitivity of surface urban energy and water balance scheme (SUEWS) to downscaling of reanalysis forcing data. Urban Clim. https://doi.org/10.1016/j.uclim.2017.05.001.

Kormann, R., Meixner, F.X., 2001. An analytical footprint model for non-neutral stratification. Bound.-Layer Meteorol. 99, 207–224.

Kusaka, H., Kondo, H., Kikegawa, Y., Kimura, F., 2001. A simple single-layer urban canopy model for atmospheric models: comp. multi-layer slab models. Bound.-Layer Meteorol. 101, 329–358. https://doi.org/10.1023/A:1019207923078.

Lau, K., Lindberg, F., Rayner, D., Thorsson, S., 2014. The effect of urban geometry on mean radiant temperature under future climate change: a study of three European cities. Int. J. Biometeorol. 59 (7), 799–814.

Lau, K.K.-L., Ren, C., Ho, J., Ng, E., 2016. Numerical modelling of mean radiant temperature in high-density sub-tropical urban environment. Energy Build. 114, 80–86.

Lawrence, D.M., Oleson, K.W., Flanner, M.G., Thornton, P.E., Swenson, S.C., Lawrence, P.J., Zeng, X., Yang, Z.L., Levis, S., Sakaguchi, K., Bonan, G.B., Slater, A.G., 2011. Parameterization improvements and functional and structural advances in version 4 of the Community Land Model. J. Adv. Model. Earth Syst. 3, 1–27. https://doi.org/10.1029/2011MS000045.

Lindberg, F., Grimmond, C.S.B., 2010. Continuous sky view factor maps from high resolution urban digital elevation models. Clim. Res. 42, 177–183.

Lindberg, F., Grimmond, C.S.B., 2011a. The influence of vegetation and building morphology on shadow patterns and mean radiant temperature in urban areas: model development and evaluation. Theor. Appl. Climatol. 105 (3), 311–323.

Lindberg, F., Grimmond, C.S.B., 2011b. Nature of vegetation and building morphology characteristics across a city: influence on shadow patterns and mean radiant temperatures in London. Urban Ecosyst. 14 (4), 617–634.

Lindberg, F., Holmer, B., Thorsson, S., 2008. SOLWEIG 1.0 — modelling spatial variations of 3D radiant fluxes and mean radiant temperature in complex urban settings. Int. J. Biometeorol. 52, 697–713.

Lindberg, F., Grimmond, C.S.B., Yogeswaran, N., Kotthaus, S., Allen, L., 2013a. Impact of city changes and weather on anthropogenic heat flux in Europe 1995–2015. Urban Clim. 4, 1–15.

Lindberg, F., Holmer, B., Thorsson, S., Rayner, D., 2013b. Characteristics of the mean radiant temperature in high latitude cities—implications for sensitive climate planning applications. Int. J. Biometeorol. 58 (5), 613–627.

Lindberg, F., Jonsson, P., Honjo, T., Wästberg, D., 2015b. Solar energy on building envelopes - 3D modelling in a 2D environment. Sol. Energy 115, 369–378.

Lindberg, F., Grimmond, C.S.B., Martilli, A., 2015a. Sunlit fractions on urban facets - impact of spatial resolution and approach. Urban Clim. 12, 65–84. https://doi.org/10.1016/j.uclim.2014.11.006.

Lindberg, F., Onomura, S., Grimmond, C.S.B., 2016a. Influence of ground surface characteristics on the mean radiant temperature in urban areas. Int. J. Biometeorol. 60 (9), 1439–1452.

Lindberg, F., Lau, K., Rayner, D., Thorsson, S., 2016b. The impact of urban planning strategies on heat stress in a climate-change perspective. Sustain. Cities Soc. 25, 1–12.

Macdonald, R., Griffiths, R., Hall, D., 1998. An improved method for the estimation of surface roughness of obstacle arrays. Atmos. Environ. 32, 1857–1864.

Masson, V., Le Moigne, P., Martin, E., Faroux, S., Alias, A., Alkama, R., Belamari, S., Barbu, A., Boone, A., Bouyssel, F., Brousseau, P., Brun, E., Calvet, J.C., Carrer, D., Decharme, B., Delire, C., Donier, S., Essaouini, K., Gibelin, A.L., Giordani, H., Habets, F., Jidane, M., Kerdraon, G., Kourzeneva, E., Lafaysse, M., Lafont, S., LebeaupinBrossier, C., Lemons, A., Mahfouf, J.-F., Marguinaud, P., Mokhtari, M., Morin, S., Pigeon, G., Salgado, R., Seity, Y., Taillefer, F., Tanguy, G., Tulet, P., Vincendon, B., Vionnet, V., Voldoire, A., 2013. The SURFEXv7.2 land and ocean surface platform for coupled or offline simulation of earth surface variables and fluxes. Geosci. Model Dev. 6, 929–960.

Masson, V., Marchadier, C., Adolphe, L., Aguejdad, R., Avner, P., Bonhomme, M., Bretagne, G., Briottet, X., Bueno, B., de Munck, C., Doukari, O., Hallegatte, S., Hidalgo, J., Houet, T., Le Bras, J., Lemonsu, A., Long, N., Moine, M.-P., Morel, T., Nolorgues, Pigeon, L.G., Salagnac, J.-L., Viguié, V., Zibouche, K., 2014. Adapting cities to climate change: a systemic modelling approach. Urban Clim. 10, 407–429.

Mayer, H., Höppe, P., 1987. Thermal comfort of man in different urban environments. Theor. Appl. Clim. 38, 43–49.

Meehl, G.A., Tebaldi, C., 2004. More intense, more frequent, and longer lasting heat waves in the 21st century. Science 305 (5686), 994–997.

Micu, D., 2012. Cold waves in the Romanian Carpathians, an indicator of negative temperature extremes. In: Air and Water Components of the Environment Conference. http://aerapa.conference.ubbcluj.ro/2012/pdf/13%20D%20Micu.pdf.

Millward-Hopkins, J., Tomlin, A., Ma, L., Ingham, D., Pourkashanian, M., 2011. Estimating aerodynamic parameters of urban-like surfaces with heterogeneous building heights. Bound-Layer Meteorol. 141, 443–465.

Nordbo, A., Karsisto, P., Matikainen, L., Wood, C.R., Järvi, L., 2015. Urban surface cover determined with airborne lidar at 2 m resolution - implications for surface energy balance modelling. Urban Clim. 13, 52–72.

Onomura, S., Grimmond, C.S.B., Lindberg, F., Holmer, B., Thorsson, S., 2015. Meteorological forcing data for urban outdoor thermal comfort models from a coupled convective boundary layer and surface energy balance scheme. Urban Clim. 11, 1–23.

ONS, 2011. Population Office for National Statistics. Residents, Workplace and Daytime Population — UK 2001 National Census [Online] Available from: https://www.nomisweb.co.uk/census/2011. (Accessed 25 February 2013).

Ordnance_Survey, 2010. Crown Database Right 2010. An Ordnance Survey/EDINA Supplied Service.

Paton, F.L., Dandy, G.C., Maier, H.R., 2014. Integrated framework for assessing urban water supply security of systems with non-traditional sources under climate change. Environ. Model. Softw. 60, 302–319.

QGIS Development Team, 2017. QGIS Geographic Information System. Open Source Geospatial Foundation Project. http://www.qgis.org/.

Rafael, S., Martins, H., Sá, E., Carvalho, D., Borrego, C., Lopes, M., 2016. Influence of urban resilience measures in the magnitude and behaviour of energy fluxes in the city of Porto (Portugal) under a climate change scenario. Sci. Total Environ. 566–567, 1500–1510.

Ratti, C.F., Richens, P., 1999. Urban texture analysis with image processing techniques. In: Proceedings of the CAADFutures99 (Atlanta, GA).

Ratti, C.F., Richens, P., 2004. Raster analysis of urban form. Environ. Plann B Plann Des. 31, 297–309.

Raupach, M., 1994. Simplified expressions for vegetation roughness length and zero-plane displacement as functions of canopy height and area index. Bound-Layer Meteorol. 71, 211–216.

Ren, C., Ng, E., Katzschner, L., 2011. Urban climatic map studies: a review. Int. J. Climatol. 31 (15), 2213–2233.

Robinson, P.J., 2001. On the definition of a heat wave. J. Appl. Meteor. 40, 762–775, 10.1175/1520-0450(2001)040<0762:OTDOAH>2.0.CO;2.

Saagi, R., Flores-Alsina, X., Kroll, S., Gernaey, K.V., Jeppsson, U., 2017. A model library

for simulation and benchmarking of integrated urban wastewater systems. Environ. Model. Softw. 93, 282–295.

Sailor, D.J., 2011. A review of methods for estimating anthropogenic heat and moisture emissions in the urban environment. Int. J. Climatol. 31 (2), 189–199.

Schoetter, R., Caiaux, J., Douville, H., 2014. Changes of western European heat wave characteristics projected by the CMIP5 ensemble. Clim. Dyn. 1–16.

Solecki, W., 2015. Hurricane Sandy in New York, extreme climate events and the urbanization of climate change: perspectives in the context of sub-Saharan African cities. Curr. Opin. Environ. Sustain. 13, 88–94. https://doi.org/10.1016/j.cosust.2015.02.007.

Srivastava, A.K., Rajeevan, M., Kshirsagar, S.R., 2009. Development of a high resolution daily gridded temperature data set (1969–2005) for the Indian region. Atmosph. Sci. Lett. 10, 249–254. https://doi.org/10.1002/asl.232.

Stewart, I.D., Oke, T.R., 2012. Local climate zones for urban temperature studies. Bull. Am. Meteorol. Soc. 93 (12), 1879–1900.

Thom, J.K., Coutts, A.M., Broadbent, A.M., Tapper, N.J., 2016. The influence of increasing tree cover on mean radiant temperature across a mixed development suburb in Adelaide, Australia. Urban For. Urban Green. 20, 233–242.

Thorsson, S., Lindberg, F., Björklund, J., Holmer, B., Rayner, D., 2010. Potential changes in outdoor thermal comfort conditions in Gothenburg, Sweden due to climate change: the influence of urban geometry. Int. J. Climatol. 31 (2), 324–335.

Thorsson, S., Rocklöv, J., Konarska, J., Lindberg, F., Holmer, B., Dousset, B., Rayner, D., 2014. Mean radiant temperature - a predictor of heat related mortality. Urban Clim. 10 (2), 332–345.

Vaidyanathan, A., Kegler, S.R., Saha, S.S., Mulholland, J.A., 2016. A statistical framework to evaluate extreme weather definitions from a health perspective: a demonstration based on extreme heat events. Bull. Am. Meteorol. Soc. 97 (10), 1817–1830.

Vautard, C., Gobiet, A., Jacob, D., Belda, M., Colette, A., Déqué, M., Fernández, J., GarcíaDíez, M., Goergen, K., Güttler, I., Halenka, T., Karacostas, T., Katragkou, E., Keuler, K., Kotlarski, S., Mayer, S., van Meijgaard, M., Nikulin, G., Patarčić, M., Scinocca, J., Sobolowski, S., Suklitsch, M., Teichmann, C., Warrach-Sagi, K., Wulkmeyer, C., Yiou, P., 2013. The simulation of European heat waves from an ensemble of regional climate models within the EURO-CORDEX project. Clim. Dyn. 41, 2555–2575. https://doi.org/10.1007/s00382-013-1714-z.

Ward, H.C., Grimmond, C.S.B., 2017. Assessing the impact of changes in surface cover, human behaviour and climate on energy partitioning across Greater London. Landsc. Urban Plan. 165, 142–161. https://doi.org/10.1016/j.landurbplan.2017.04.001.

Ward, H.C., Kotthaus, S., Järvi, L, Grimmond, C.S.B., 2016. Surface urban energy and water balance scheme (SUEWS): development and evaluation at two UK sites. Urban Clim. 18, 1–32. https://doi.org/10.1016/j.uclim.2016.05.001.

Ward, H.C., Tan, Y., Gabey, A.M., Kotthaus, S., Morrison, W.T.J., Grimmond, C.S.B., 2017a. Impact of temporal resolution of precipitation forcing data on modelled urban-atmosphere exchanges and surface conditions. Int. J. Climatol. https://doi.org/10.1002/joc.5200.

Ward, H.C., Järvi, L., Sun, T., Onomura, S., Lindberg, F., Olofson, F., Gabey, A., Grimmond, C.S.B., 2017b. SUEWS Manual V2017b. Department of Meteorology, University of Reading, Reading, UK. http://urban-climate.net/umep/SUEWS.

Watson, I.D., Johnson, G.T., 1987. Graphical estimation of sky view-factors in urban environments. J. Climatol. 7, 193–219.

Weedon, G.P., Gomes, S., Viterbo, P., Shuttleworth, W.J., Blyth, E., Österle, H., Adam, J.C., Bellouin, N., Boucher, O., Best, M., 2011. Creation of the WATCH Forcing data and its use to assess global and regional reference crop evaporation over land during the twentieth century. J. Hydrom. 12, 823–848.

Weedon, G.P., Balsamo, G., Bellouin, N., Gomes, S., Best, M., Viterbo, P., 2014. The WFDEI meteorological forcing data set: WATCH Forcing Data methodology applied to ERA-Interim reanalysis data. Water Resour. Res. 50, 7505–7514.

Wilby, R.L., Hay, L.E., Gutowski Jr., W.J., Arrit, R.W., Takle, E.S., Pan, Z., Leavesley, G.H., Clark, M.P., 2000. Hydrological responses to dynamically and statistically downscaled climate model output. Geophys. Res. Lett. 27, 1199–1202.